COMPONENTS OF DETECTOR RESPONSE FUNCTION: EXPERIMENT AND MONTE CARLO SIMULATIONS

A THESIS SUBMITTED TO
THE GRADUATE SCHOOL OF NATURAL AND APPLIED SCIENCES
OF
MIDDLE EAST TECHNICAL UNIVERSITY

BY

RENGİN PEKÖZ

IN PARTIAL FULFILLMENT OF THE REQUIREMENTS

FOR

THE DEGREE OF MASTER OF SCIENCE

IN

PHYSICS

AUGUST 2004

Approval of the Graduate School of Natural and Applied Sciences.

Prof. Dr. Canan Özgen
Director

I certify that this thesis satisfies all the requirements as a thesis for the degree of Master of Science.

Prof. Dr. Sinan Bilikmen
Head of Department

This is to certify that we have read this thesis and that in our opinion it is fully adequate, in scope and quality, as a thesis for the degree of Master of Science.

Prof. Dr. Cüneyt Can
Supervisor

Examining Committee Members

Prof. Dr. Pervin Arıkan (Gazi University, PHYS) _____

Prof. Dr. Cüneyt Can (METU, PHYS) _____

Prof. Dr. Bülent Akınoğlu (METU, PHYS) _____

Prof. Dr. Raşit Turan (METU, PHYS) _____

Assist. Prof. Dr. Bayram Tekin (METU, PHYS) _____

I hereby declare that all information in this document has been obtained and presented in accordance with academic rules and ethical conduct. I also declare that, as required by these rules and conduct, I have fully cited and referenced all material and results that are not original to this work.

Rengin Peköz

ABSTRACT

COMPONENTS OF DETECTOR RESPONSE FUNCTION:
EXPERIMENT AND MONTE CARLO SIMULATIONS

PEKÖZ, RENGİN

M.S., Department of Physics

Supervisor: Prof. Dr. Cüneyt Can

AUGUST 2004, 55 pages

Components of the response function of a high-purity germanium (HPGe) detector due to full or partial energy deposition by gamma- and X-rays were studied. Experimental response functions for ^{241}Am, Ba and Tb were compared with those obtained from the Monte Carlo simulations. The role of physical mechanisms for each component was investigated by considering escape/absorption of photons, photoelectrons, Auger electrons, recoil electrons and X-rays of the detector material. A detailed comparison of the experimental Compton, photoelectron, detector X-ray escape components and full-energy peaks with those obtained from Monte Carlo program are presented.

Keywords: Photoelectron escape, Compton escape, X-ray escape, HPGe detector, Monte Carlo.

ÖZ

DEDEKTÖLERİN TEPKİ FONKSİYONLARININ ELEMANLARI: DENEY VE MONTE CARLO SİMÜLASYONLARI

PEKÖZ, RENGİN
Yüksek Lisans, Fizik Bölümü
Tez Yöneticisi: Prof. Dr. Cüneyt Can

AĞUSTOS 2004, 55 sayfa

Bir HPGe dedektörünün, gama ve X-ışınlarının tam ya da kısmi enerji depolaması nedeniyle oluşan tepki fonksiyonlarının elemanları çalışıldı. ^{241}Am, Tb ve Ba'nın deneysel tepki fonksiyonları, Monte Carlo simülasyonundan elde edilen sonuçlarla karşılaştırıldı. Her eleman için fiziksel mekanizmaların rolü, fotonların, fotoelektronların, Auger elektronlarının, geri tepen elektronların ve dedektör maddesinin X-ışınlarının kaçma/soğurulma durumları düşünülerek araştırıldı. Deneysel Compton, fotoelektron, dedektör X-ışını kaçağı elemanlarının ve tam-enerji piklerinin, Monte Carlo programından elde edilen sonuçlarla detaylı karşılaştırması yapıldı.

Anahtar Sözcükler: Fotoelektron kaçağı, Compton kaçağı, X-ışını kaçağı, HPGe dedektörü, Monte Carlo.

To My Family...

ACKNOWLEDGMENTS

The work presented in this thesis would not have been possible without the involvement of a number of people. I would like to thank the following persons in particular:

I would like to express my deepest gratitude to my supervisor Prof. Dr. Cüneyt Can for his help, attitude, encouragement, guidance and insight throughout this research.

I would like to express my sincere gratitude to Dr. Ercan Yılmaz for his invaluable help and friendly attitude.

I would like to thank all the secretaries of Dean's Office for their help and friendly behaviors.

There are no words to describe the appreciation and gratitude I feel for my family. I thank them for their optimism, beautiful spirits and belief in me.

I would like to thank to Vedat Tanrıverdi, Ayşe Küçükarslan, Orhan Karabulut, Emre Taşçı, and to my other friends for their help and encouragement.

TABLE OF CONTENTS

LIST OF TABLES

LIST OF FIGURES

CHAPTER 1

INTRODUCTION

Semiconductor detectors are used in basic science (astrophysics, atomic and nuclear physics), applied science (material analysis, medical imaging and synchrotron research) and industrial science (XRF analysis and quality control). Therefore, the energy resolution, efficiency and the detailed shape of the response function of a detector are parameters of interest for elemental analysis and fundamental research.

An X-ray or gamma-ray photon is uncharged and creates no direct ionization or excitation of the matter through which it passes. The detection of X-rays and gamma-rays is therefore critically dependent on how these photons undergo interaction in the detector, so that electrically charged particles are created. The electric signal is picked up from the detector electrode and processed by a complex electronics and/or software package. X-ray or gamma-ray spectrum thus obtained is called detector response function or pulse height distribution.

Over the years scientists have developed various techniques to study response function of detectors. Response functions can be generated by one of three different methods [1]:

1. Experimental: The pulse height spectra resulting from a large number of

monoenergetic sources are measured. A response matrix as a function of pulse height is formed and interpolated for other energies.

2. Monte Carlo: Response function is obtained by modelling the energy deposition within the detector resulting from all major mechanisms by simulation for a large number of photons.

3. Semi-empirical: The various features of the measured spectra from single energy sources are fitted by analytical functions and the best (least-squares) estimates of the parameters in the fitting functions are obtained, and then these parameters are obtained as a function of source energy.

All of these methods have advantages and disadvantages. The experimental and semi-empirical methods are more direct than the Monte Carlo method, but they require the availability of either a large or small number of monoenergetic sources covering the range of interest for the source energy. Monte Carlo method gives the user more insight into the physics of spectrometry than the other two methods which are based on experimental data. On the other hand, Monte Carlo method requires a good understanding of the geometry and and the physical mechanisms for the operation of the detector which is often difficult to determine.

The reason for this wide range of interest in semiconductor detectors is that the combined effect of the interactions of the incident photons, through which they deposit all or part of their energies with the detector is quite complicated. The major mechanisms involve interaction of primary radiation with the detector material, and interaction of characteristic X-rays, photoelectrons and Auger

electrons in the detector. A typical X-ray or gamma-ray spectrum contains a wealth of information, including one or more full-energy peaks (FEP) and their associated low-energy tailings, and escape components due to loss of photons and electrons. The role of electrons to and from electrical contact materials and the effect of dead layer have also been studied extensively.

Until recently, mainly silicon-based detectors, that is, Si(Li), have been used in low-energy X-ray detection, and many researchers have studied to improve the understanding of the detector response function experimentally [2-5], theoretically [6-10] and semi-empirically [11-14].

However, the presently available high-purity germanium (HPGe) detectors show significant improvements in manufacturing technology [15]. The dead layer of HPGe detectors have been significantly reduced enabling these devices to detect lower energies. Furthermore, because of the intrinsic properties of the germanium material, the resolution of these detectors are better than the traditional silicon detectors. Thus, it is of interest for some authors [16-19] to determine the HPGe detector response function and compare it with those types of detectors.

The escape of characteristic X-rays, that is, X-rays of the detector material, has been studied in detail, both experimentally and by analytical calculations and simulations. The physical mechanism for escape of X-rays is simple and the energy of an escape peak is well defined. However, escape peaks may cause problems in qualitative as well as in quantitative analysis of X-ray spectra. Complete or partial overlap of escape peaks with gamma or X-ray peaks may lead to misinterpretations of spectra. In an earlier, but often-cited study [20], it was shown

that the experimental measurements of the relative intensity of the K_α and K_β escape peak produced in an intrinsic Ge detector agreed quite well with the calculated intensities. Can and Bilgici [21] studied the effect of the solid angle for the incident photons on the escape probability of Ge K X-rays using collimators with varying apertures for 59.5 keV photons incident on an HPGe detector, and demonstrated the importance of escape from the side surface of the detector. They also verified this by the Monte Carlo simulations.

The escape of Compton-scattered photons has been investigated by Martin and Burns [22], and Pašić and Ilakovac [23] using an ^{241}Am source and an HPGe detector. These experiments have shown the importance of escape of primary photons undergoing predominantly single 180° scattering.

In the last decade, attention has shifted to escape of photoelectrons, with the aim to determine the exponential tail and flat shelf on the low-energy side of FEPs. According to many authors [1, 24, 25], the so-called exponential tail on the low-energy side of the FEP is due to effects of incomplete charge collection (ICC). Various physical mechanisms in the detector's components (crystal, contact layer) such as the transport of the photo- and Auger electrons or the diffusion of thermalized electrons are known as the reasons for the ICC. The other contributing factors to low-energy tail are the bias applied, the thickness and the type of the contact layer, and the dead layer.

Recent experimental investigations revealed the existence of a step-like, or shelf-like, feature with definite cut-off energies in Si(Li) and Ge detectors. When an incoming photon interacts with a silicon atom, the emission of a photoelectron

together with K and L Auger electrons occurs. Then, the energy loss due to electron escape through the front surface can vary from zero to the full photon energy. This process results in a flat shelf that extends from the FEP down to zero energy. Alternatively, the interaction of an incoming photon results in emission of a photoelectron and a Si K X-ray. If X-ray escapes, there will be a shelf extending from the Si escape peak down to zero energy. However, if the photoelectron escapes and the K X-ray is detected, then the shelf will extend from 1.74 keV (Si K-shell binding energy) up to the full energy of the incident photon. This process causes a step (*i.e.* cut-off) at 1.74 keV energy in the spectrum. The spectra for HPGe detectors have similar features except for the absence of the low-energy tailing, which is highly dependent on the detector technology, and the position of the cut-off (at 11.1 keV) and the energy of Ge X-ray escape peak.

The shelf-like structure in a Si(Li) detector was first reported by Campbell *et al.* [3] using Mn K X-rays from a ^{55}Fe source. Since then, a number of studies were published regarding the source and physical features of the shelf [4,5,8,17-19,26-28]. One of the most important aspects of the shelf structure is the actual shape of the continuous spectrum extending to the full-energy peak. Height and intensity of a shelf are usually crucial in estimating the significance of photoelectron escape. Effects of pulse processing time, diffusion loss of "hot" electrons produced by photoelectrons and Auger electrons, and the role of contact material and detector dead layer have been studied with a lot of success by Campbell *et al.* [3].

However, until recently, nobody questioned the "flatness" of a shelf. Since the

probability of photoelectron escape is highly dependent on the depth at which they are produced, photoelectrons closer to a surface, usually the front end, of the detector can escape more easily, but will deposit a small amount of energy. On the other hand, photoelectrons from the deeper regions of the detector will deposit more energy, but the probability of escape will be much smaller. Therefore, the intensity profile of photoelectron escape is expected to have a slope rather than a flat structure. Lowe's [16] analytical calculations for photons with 5.9 keV energy incident on a Si(Li) and HPGe detector indicated such a behavior for both photoelectrons and Auger electrons. Lately, Papp [18] reported that the so-called flat plateau had a slope in both Si(Li) and HPGe detectors.

Experimental studies of response functions at METU started a few years ago when Can [27] measured the response function of a planar HPGe detector due to escape of photoelectrons, Compton-scattered photons and Ge X-rays for a ^{241}Am point source with 59.5 keV energy. The main difference of this study from the earlier works was that all three escape mechanisms were observed in the same experiment. The results of this investigation indicated that the escape of scattered photons and photoelectrons could be more important than the escape of Ge X-rays for the efficiency of a detector. Moreover, in this study, a hump-like structure was reported for the photoelectron escape with much of intensity in the 11-25 keV range. Recently, Yılmaz *et al.* [28, 29] investigated the escape of Ge X-rays, photoelectrons and 180° Compton-scattered photons for incident X-rays in the energy range 8-52 keV and gamma-rays of 81 keV energy. The photoelectron escape profiles they obtained displayed more or less the same behavior as in

the ^{241}Am spectrum. Apart from these experimental studies, a Monte Carlo program was also developed at METU. Good agreement was obtained between the results of the experiment and the Monte Carlo simulations for the escape of Ge K X-rays and Compton-scattered photons. However, the simulations have always underestimated the photoelectron escape.

In order to gain insight into the physical mechanisms responsible for the escape components, we simulated the response function of our HPGe detector at three different energies, 32, 44.2 and 59.5 keV, with particular emphasis on photoelectron transport mechanism. We showed that there is a slope in the photoelectron escape component, but not a hump-like structure as was seen in our experiments. We also demonstrated the existence of another mechanism for the photoelectron escape in coincident with Ge X-ray escape. The quasi-spectra obtained from the simulations will be compared with the experimental response functions for Ba and Tb X-rays, and ^{241}Am gamma rays.

Another interesting part of our study was the assessment of the importance of multiple scattering followed by photoelectric absorption. The contribution to FEP intensity from coherent or Compton scattering events followed by photoelectric absorption was calculated by O'Meara and Campbell [30] using Monte Carlo method, and found to be significant for incident photon energies above 30 keV. At MeV energies, Sood and Gardner [1] recently studied, among other things, the Doppler broadened continuum broken into first, second and third Compton scattering events. In the present thesis, we recorded the energy of the recoil electron(s), assumed to be fully deposited in the detector, with the condition that

the scattered photon eventually underwent a photoelectric interaction. Since the amount of deposited energy by recoil electrons directly effects the intensity and the low-energy tailing of FEP, we investigated the contribution of single and multiple scattering to the response function in detail.

This thesis is organized as follows: in the second chapter, the theory of interaction of radiation with matter is given. In the third chapter, the experimental set-up and the features of ^{241}Am gamma-, and Tb and Ba X-ray spectra are discussed. In the fourth chapter, the basic principles and the present application of the Monte Carlo simulation are given. Finally, in the fifth chapter, the experimental spectra are presented and compared with the Monte Carlo simulations.

CHAPTER 2

THEORY

2.1 Interaction of Radiation with Matter

Although a large number of interaction mechanisms are possible for radiation in matter, only four major types play an important role in measurements: photoelectric effect, Compton (incoherent) scattering, coherent (Rayleigh) scattering, and pair production. All these processes lead to the partial or full transfer of the photon energy to electron energy. Contrary to the continuous slowing down of charged particles, photons either disappear or are scattered as they pass through matter. The mass attenuation coefficient for the individual interactions and the sum of the first three processes for Germanium are shown in Fig. 2.1 [31]. It can be seen that in the energy range 32-59.5 keV considered in our studies, the major interaction is photoelectric absorption while the total of the other two scattering processes is about $4 - 12\%$ of the total cross-section.

2.1.1 Photoelectric Effect

One of the interactions is the photoelectric effect in which the incident photon disappears and in its place, an electron is produced from one of the electron shells of the absorber atom. The kinetic energy, E_{pe}, of this electron is given by the

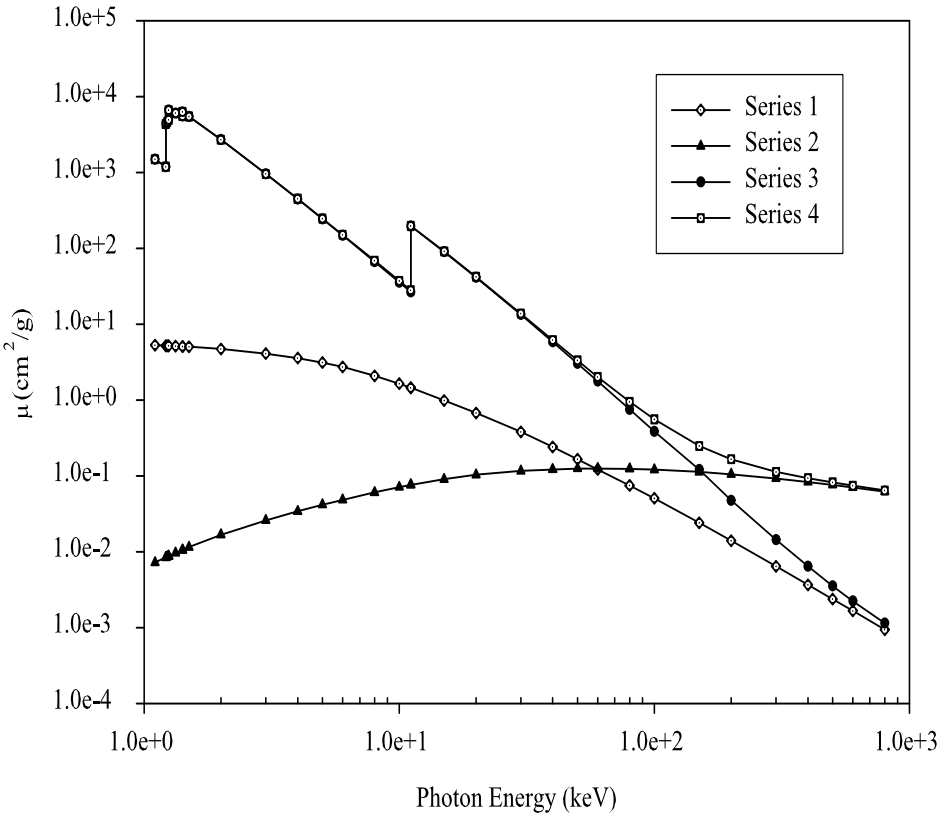

Figure 2.1: *Mass attenuation coefficients for photons in Germanium.* Series1 (coherent scattering), Series2 (incoherent scattering), Series3 (photoelectric absorption) and Series4 (total attenuation).

incident photon energy, $E_0 = h\nu$, minus the binding energy, E^b, of the electron in its original shell. Electrons thus ejected from atoms are called photoelectrons. This process is shown in Fig. 2.2.

The interaction is with the atom as a whole and cannot take place with free electrons. The most probable origin of the photoelectron is the most tightly bound or K-shell of the atom for photons of sufficient energy. Since these photoelectrons are produced by a process which completely absorbs the energy of the

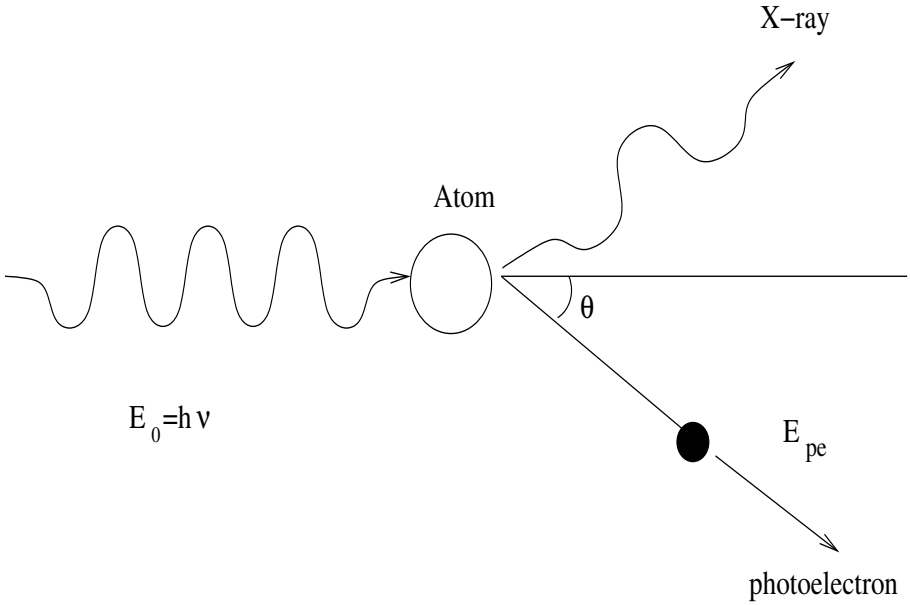

Figure 2.2: *Photoelectric effect.*

incident photon, they may carry considerable kinetic energy. This means that photoelectrons themselves become a source of ionization, if they pass close to neighboring atoms they strip off electrons from them. The photoelectric process is the predominant mode of interaction for gamma-rays (or X-rays) of relatively low energy. The process is also enhanced for absorber materials of high atomic number Z.

The vacancy that is created in the electron shell because of the removal of an electron through this process will be filled by an electron from a less tightly bound state. This vacancy is often filled by electrons from the outer shells of the atom with the emission of a characteristic X-ray photon. The characteristic X-ray energy is equal to the difference in binding energy between the participating inner

and outer electron shells or subshells. Because of this reason, a characteristic X-ray spectrum consists of a number of discrete lines, each corresponding to one of many transition probabilities as shown in Fig. 2.3.

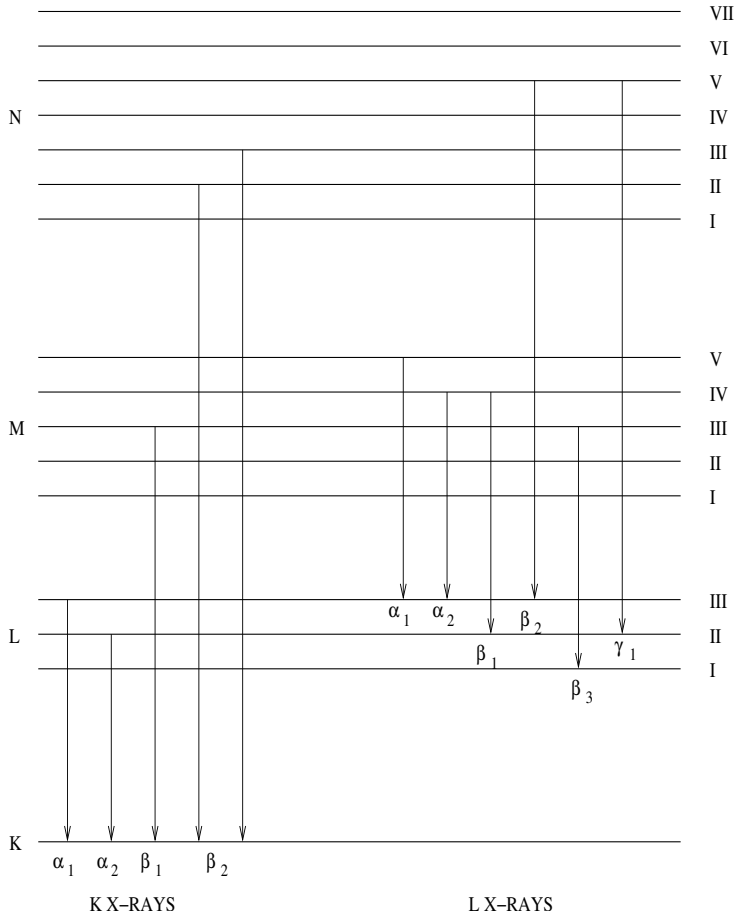

Figure 2.3: *Atomic energy levels involved in the emission of X-rays.*

Alternatively, the excitation energy may cause the simultaneous emission from the atom of a second electron, called an Auger electron, from another less tightly bound state. An inner vacancy can be followed by a great number of different Auger transitions as shown in Fig. 2.4 [32]. The energy of an Auger electron is given by the difference between the original atomic excitation energy and the

binding energy of the shell from which the electron was ejected. The ejection of an Auger electron is a competitive process to the emission of characteristic X-rays for an atom in an excited state. The fluorescence yield, *i.e.* ω_i in which i refers to the electron shell or subshell from which the primary photoelectron was removed, is defined as the fraction of all cases in which the excited atom emits a characteristic X-ray photon in its deexcitation.

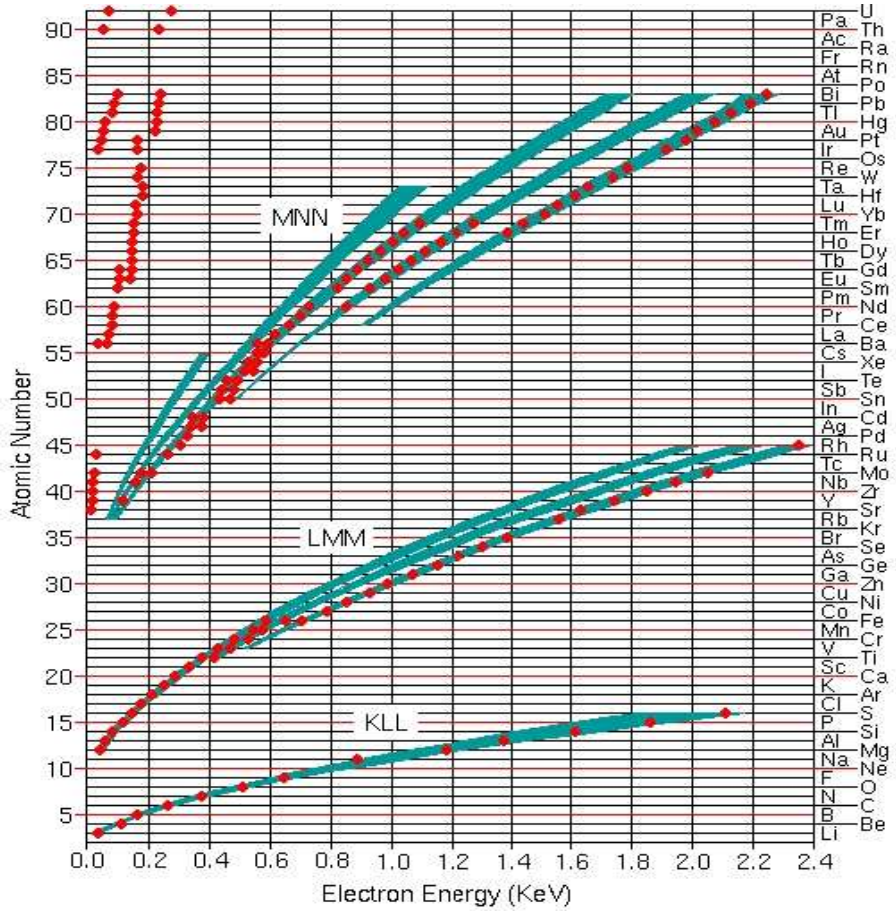

Figure 2.4: *Auger spectral transitions through Z=92.*

The angular distribution of the photoelectrons is given by [33]

$$dn = \frac{\sin^2\theta}{(1-\beta\cos\theta)^4} d\Omega \tag{2.1}$$

where dn is the number of photoelectrons ejected in the small solid angle $d\Omega$ making an angle θ with the incoming photon and $\beta = v/c$ for the ejected electron. The second term in the denominator can be neglected at low-photon energies, and we then have a $\sin^2\theta$ distribution which shows a maximum at right angles to the photon direction. As the photon energy increases, the angular distribution tends to maximize more and more in the forward direction.

Photoelectron loses its energy in ionizing and radiative collisions as it passes through matter and in each of these it may suffer significant deflections. In addition, elastic scattering results a large number of deflections. The range, R, of an electron is an experimental concept, relating to the thickness of an absorber which the particle can just penetrate. Several distinct definitions of range, which depend upon the method employed to determine them, are in common usage. They all relate, however, to roughly the same quantity. It must be recognized that the electron's total path length is a quantity which is completely different from its range. The total path length is measured along the actual path of the electron, while the range is the maximum distance reached in the initial direction of the electron.

Bethe [34] has developed expressions for the stopping power of electrons. The energy deposited within the absorber can be calculated from

$$\triangle E_{pe} = \left(-\frac{dE_{pe}}{dx}\right)_{avg} t \tag{2.2}$$

where t is the absorber thickness and $(-dE_{pe}/dx)_{avg}$ is the linear stopping power averaged over the energy of the particle while in the absorber.

Bremsstrahlung production now becomes important, and so two equations are needed to account for the total linear stopping power for electrons. It is the sum of the collisional (excitation and ionization) and radiative losses:

$$\frac{dE_{pe}}{dx} = \left(\frac{dE_{pe}}{dx}\right)_{coll} + \left(\frac{dE_{pe}}{dx}\right)_{rad}. \tag{2.3}$$

The first term on the right of the above equation is due to the collisional energy loss given by [34]

$$\begin{aligned} -\left(\frac{dE_{pe}}{dx}\right)_{coll} &= \frac{2\pi e^4 NZ}{m_0 v^2} \ln \frac{m_0 v^2 E_{pe}}{2I^2(1-\beta^2)} - (\ln 2)(2\sqrt{1-\beta^2} - 1 + \beta^2) \\ &\quad +(1-\beta^2) + \frac{1}{8}(1-\sqrt{1-\beta^2})^2. \end{aligned} \tag{2.4}$$

The second term in the Eqn. 2.3 is the linear specific energy loss through this radiative process given by

$$-\left(\frac{dE_{pe}}{dx}\right)_{rad} = \frac{NE_{pe}Z(Z+1)e^4}{137m_0^2c^4}\left(4\ln\frac{2E_{pe}}{m_0c^2} - \frac{4}{3}\right). \tag{2.5}$$

In Eq. (2.4) and (2.5), v and e are the velocity and charge of the primary particle, N and Z are the number density and atomic number of the absorber atoms, m_0 is the electron rest mass, e is the electronic charge, and I is the average excitation and ionization potential of the absorber. The presence of E_{pe} and Z^2 in the numerator of Eq. (2.5) shows the increasing importance of radiation losses at high energies and in absorbers of high atomic number.

The ratio of the specific energy losses is given approximately by

$$\frac{(dE_{pe}/dx)_{rad}}{(dE_{pe}/dx)_{coll}} \cong \frac{E_{pe}Z}{700} \tag{2.6}$$

where E_{pe} is in units of MeV. For the photoelectrons of interest here, typical energies are less than 0.1 MeV. Therefore, radiative losses are always a very small fraction of the energy losses due to ionization and excitation.

2.1.2 Compton Scattering

In Compton scattering, the incoming photon is deflected through an angle θ with respect to its original direction as seen in Fig. 2.5. The photon transfers a portion of its energy to the electron (assumed to be initially at rest), which is known as the recoil electron.

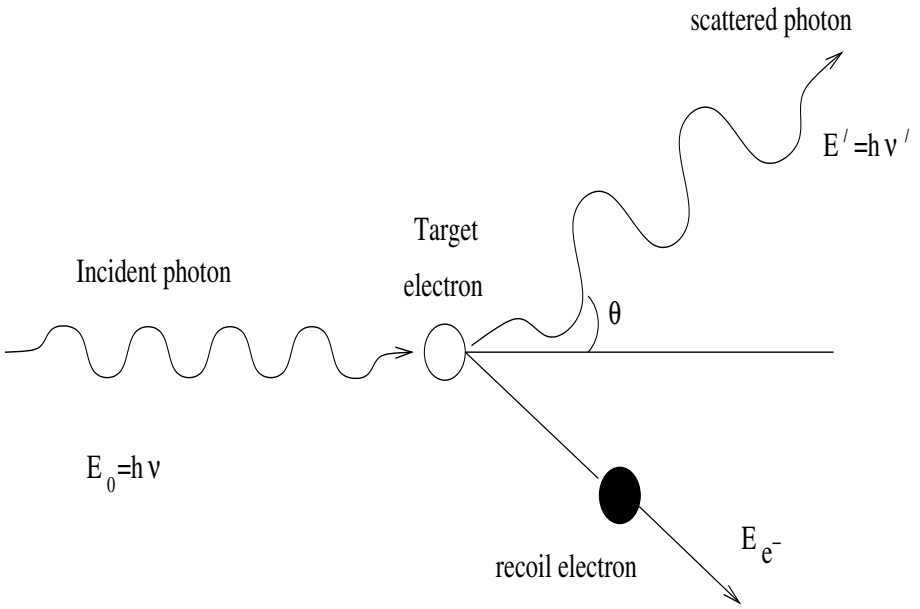

Figure 2.5: *Compton scattering.*

The expression that relates the energy transfer and the scattering angle for any given interaction can simply be derived by writing simultaneous equations for the conservation of energy and momentum. Using the symbols defined in the

Fig. 2.5, we can show that

$$\begin{aligned} E' &= h\nu' \\ &= \frac{h\nu}{1 + ((h\nu)/(m_0c^2))(1 - \cos\theta)} \end{aligned} \tag{2.7}$$

where m_0c^2 is the rest mass energy of the electron. For small scattering angles θ, very little energy is transferred. Some of the original energy is always retained by the incident photon, even in the extreme cases, which are described below. The kinetic energy of the recoil electron is therefore

$$\begin{aligned} E_{e^-} &= h\nu - h\nu' \\ &= h\nu \left(\frac{(h\nu/m_0c^2)(1 - \cos\theta)}{1 + (h\nu/m_0c^2)(1 - \cos\theta)} \right). \end{aligned} \tag{2.8}$$

Two extreme cases can be identified:

1. A grazing angle scattering, or one in which $\theta \cong 0$. In this case, Eq. (2.7) and Eq. (2.8) predict that $h\nu' \cong h\nu$ and $E_{e^-} \cong 0$. In this extreme, the recoil Compton electron has very little energy and the scattered photons has nearly the same energy as the incident photon.

2. A head-on collision in which $\theta = \pi$. In this extreme, the incident photon is backscattered towards its original direction, whereas the electron moves along the direction of incidence. This extreme represents the maximum energy that can be transferred to an electron in a single Compton interaction. Eq. (2.7) and Eq. (2.8) yield for this case:

$$E' = h\nu'|_{\theta=\pi} = \frac{h\nu}{1 + 2h\nu/m_0c^2} \tag{2.9}$$

and

$$E_{e^-}|_{\theta=\pi} = \frac{h\nu}{1 + m_0c^2/2h\nu}. \tag{2.10}$$

In normal circumstances, all scattering angles will occur in the detector. Therefore, a continuum of energies can be transferred to the electron, ranging from zero up to the maximum predicted by Eq. (2.10).

The Compton analysis gives no information about the probability of an interaction, or about the angular distribution of the scattered components. The angular distribution of scattered photons is predicted by the Klein-Nishina formula [35] for the differential scattering cross section $d\sigma/d\Omega$:

$$\frac{d\sigma}{d\Omega} = Zr_0^2 \left(\frac{1}{1+\alpha(1-\cos\theta)}\right)^2 \left(\frac{1+\cos^2\theta}{2}\right) \left(1 + \frac{\alpha^2(1-\cos\theta)^2}{(1+\cos^2\theta)[1+\alpha(1-\cos\theta)]}\right) \tag{2.11}$$

where $\alpha \equiv h\nu/m_0c^2$ and r_0 is the classical electron radius. The distribution indicates that there is a strong tendency for forward scattering at high values of the photon energy.

Electron binding must be considered at low energies and this is usually achieved by including a factor, $S(E_0, \theta, Z)$, which is the incoherent scattering function [36, 37] derived from atomic wavefunctions. This reduces the cross-section for Compton scattering for small momentum transfers, that is, for low-angle scattering, particularly at low energies

$$\left[\frac{d\sigma}{d\Omega}\right]_{incoh} = \left[\frac{d\sigma}{d\Omega}\right]_{KN} \cdot S(E_0, \theta, Z). \tag{2.12}$$

However, bound electrons are necessarily in motion and their momentum prior to interaction influences E'. This energy and p_z, the component of the electron's

momentum parallel to the scattering vector, are related by the expression [22]

$$p_z = \frac{E_0 E'(1-\cos\theta) - m_0 c^2 (E_0 - E')}{c(E_0^2 + E'^2 - 2E_0 E'\cos\theta)^{1/2}}. \tag{2.13}$$

The probability distribution $J(p_z)$, the Compton profile [38], may be used to calculate the distribution of energy of the scattered photon which is no longer uniquely defined by the scattering angle. The effect is a Doppler broadening of the Compton edge and backscattering peak that is particularly significant for large-angle scattering.

2.1.3 Coherent Scattering

In coherent scattering (also known as elastic or Rayleigh scattering), a photon that strikes an atom will be re-emitted with only a small change in its direction and with practically no loss of its energy. Even at energies of 0.1 MeV and above, coherent scattering by tightly bound atomic electrons can be significant in heavy elements. The permissible Rayleigh scattering angles are always small, because the recoil imparted to the atom must not produce atomic excitation or ionization.

The angular distribution of scattered gamma rays can be calculated from the equation [10]

$$\left(\frac{d\sigma}{d\Omega}\right)_{Th} = \frac{r_0^2}{2}(1+\cos^2\theta)\cdot[F(q,Z)]^2. \tag{2.14}$$

The factor $(r_0^2/2)(1+\cos^2\theta)$ is the differential cross-section for Thompson scattering from a single electron. F(q, Z) is the relativistic Hartree-Fock atomic form factor [37] which represents the probability that the recoil momentum q is transferred to Z electrons of an atom without any absorption.

2.1.4 Pair Production

In pair production, the photon is completely absorbed and in its place appears a positron-electron pair whose total energy is just equal to $h\nu$. Thus we write

$$h\nu = (T_- + m_0c^2) + (T_+ + m_0c^2) \tag{2.15}$$

where T_- and T_+ are the kinetic energies of the electron and positron, respectively, and m_0c^2 is the electronic rest energy [39]. Because an energy of $2m_0c^2$ is required to create the electron-positron pair, a minimum photon energy 1.02 MeV is needed to make the process energetically possible. In our experiments, the photons had a maximum energy of 59.5 keV. Therefore, pair production process was not possible.

CHAPTER 3

EXPERIMENT

3.1 Experimental Set-up

The experimental set-up used at METU to measure response functions is shown schematically in Fig. 3.1.

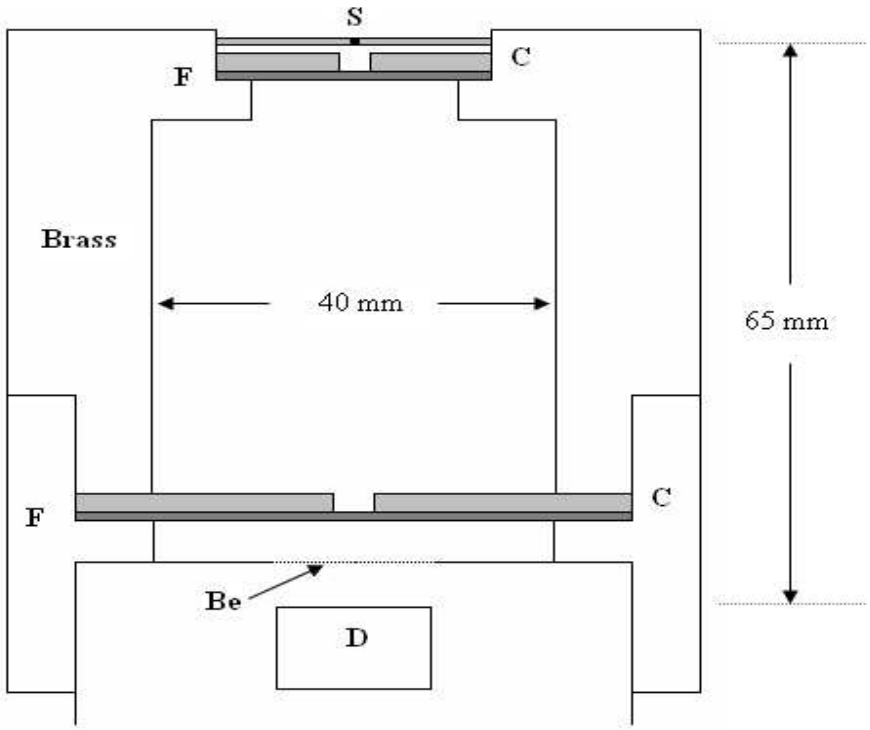

Figure 3.1: *Experimental set-up.* F: Filter, S: Source, C: Collimator, D: Detector, Be: Beryllium window (not to scale).

Even though our aim will be a qualitative and quantitative comparison of experiment and Monte Carlo simulations, we will outline the experimental techniques used, and discuss the origin and features of various components in each spectrum. Photons from an ^{241}Am point source with 59.5 keV, and Tb and Ba X-rays from a calibration source (Amersham, code AMC. 2084) were used. The photon-excited elements in the calibration source produced X-rays in the energy range 8 keV to 51.7 keV. According to the manufacturer, the planar HPGe detector (Canberra, Model 3502) had an active diameter of 16 mm, 10 mm thickness and 200 mm^2 active area. The distance between the front surface of the detector and the beryllium window was 5 mm. The source was located 65 mm above the detector on its main axis. The X-rays were collimated by a set of two 2 mm thick lead collimators, one directly below the source and the other 10 mm above the detector. The top collimator was used to minimize the number of photons reaching the detector after being scattered from the source holder, while the bottom collimator defined the desired solid angle. The spectra of ^{241}Am was taken with two filters (0.4 mm Cu and 1 mm Al) which were placed directly under the top collimator in order to eliminate the low energy peaks (Np L and M X-rays originating from the source, and x-rays from the housing of the source, the collimators, and possibly the detector contact layer) from the spectrum and revealing the components due to the escape process. The spectrum of Tb was taken with an Al filter, and a Cu filter was used for the spectrum of Ba. The components of the response function due to escape of Ge X-rays, photoelectrons and Compton-scattered photons could thus be observed. The only negative effect

of the filters was a small tailing, due to scattering, just below the FEP. Standard counting electronics and signal processing units consisting of a preamplifier, an amplifier, an oscilloscope and a multichannel pulse height analyzer were used. The response functions of the HPGe detector for incident ^{241}Am [27], Tb and Ba [28] are given in Figs. 3.2-3.4. The effect of the filters is best seen in the spectrum of ^{241}Am. Fig. 3.2 shows that the low-energy gamma rays, particularly 26.3 keV line, and Np L X-rays were almost completely absorbed by the filters. The only negative effect was the small degradation of the FEP due to scattering. The net counts under the FEP, and the X-ray, Compton and photoelectron escape peaks, after appropriate background subtraction, were determined using a peak-fitting program (Jandel Scientific, 1989).

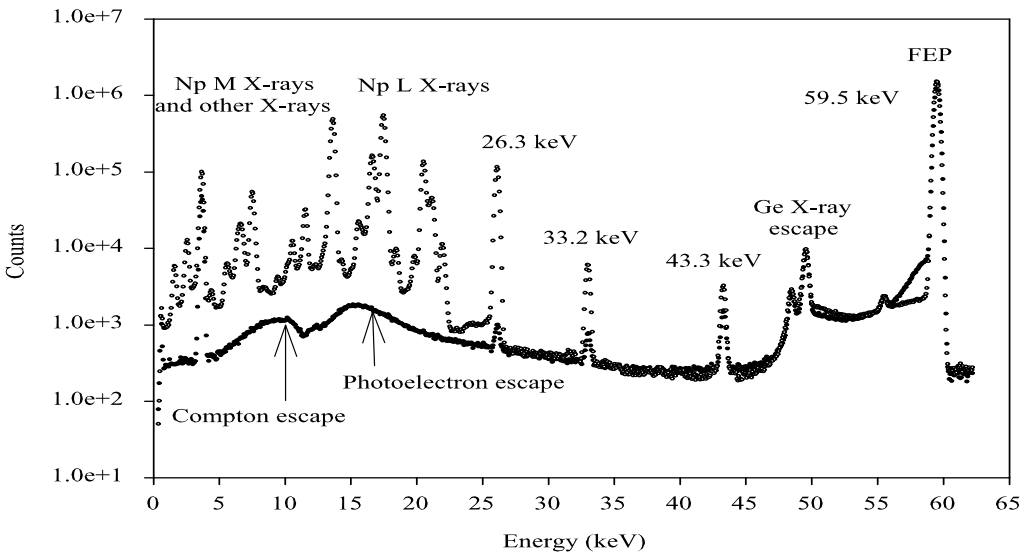

Figure 3.2: *Spectrum of* ^{241}*Am.*

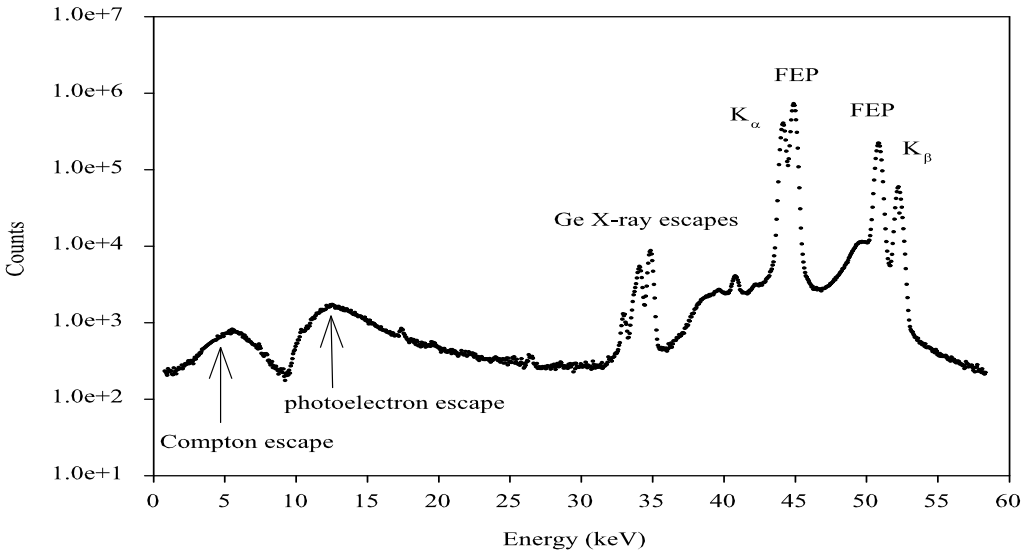

Figure 3.3: *Spectrum of Tb K X-rays.*

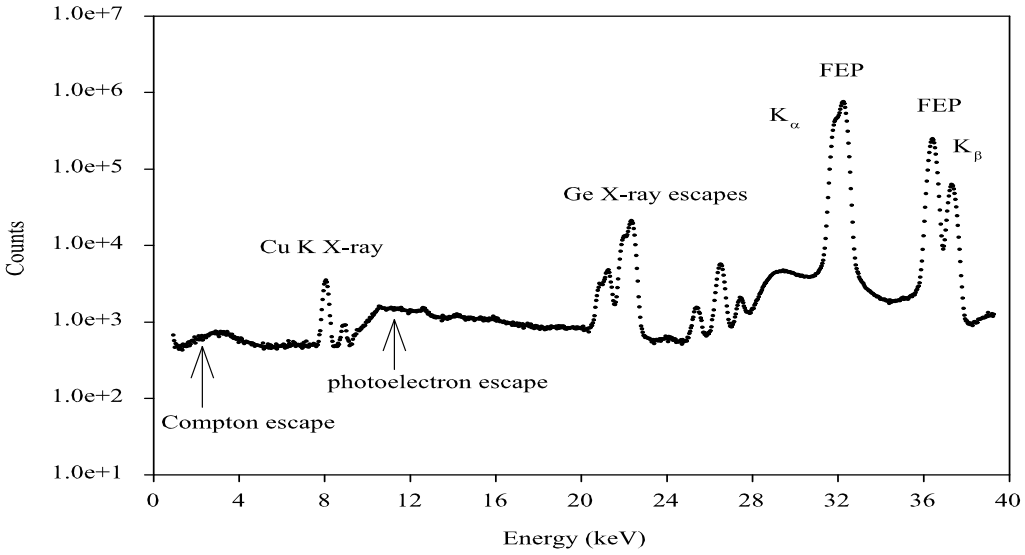

Figure 3.4: *Spectrum of Ba K X-rays.*

3.2 Spectral Features

3.2.1 Full-Energy Peaks

A photon that undergoes an interaction of any kind within the detector is expected to deposit its full energy. In this case FEPs of ^{241}Am, Tb and Ba are obtained as shown in Figs. 3.2-3.4, respectively. In the energy region 32-59.5 keV the most probable interaction between the primary radiation and the atoms of the detector material is the photoelectric absorption by the K-shell electrons of Ge. When the photoelectron and the Ge X-ray or Auger electron, produced by this interaction, deposit all of their energy in the detector, the FEPs at 32, 44.2 and 59.5 keV are observed for Ba K_α X-ray, Tb K_α X-ray and ^{241}Am gamma-ray, respectively. As can be seen from the Fig. 3.2, there is only one prominent FEP which corresponds to the incident photon energy of ^{241}Am. However, in the case of Tb and Ba, there are four FEPs which correspond to the $K_{\alpha1}$, $K_{\alpha2}$, $K_{\beta1}$, and $K_{\beta2}$ X-rays of Tb and Ba.

3.2.2 Ge X-Ray Escape

In the photoelectric absorption process, a characteristic Ge X-ray is emitted by the Ge atom. In the majority of cases, this X-ray energy is reabsorbed fairly near the original interaction site. If the photoelectric absorption occurs near a surface of the detector, however, the X-ray photon can escape. In this case, the energy deposited in the detector is decreased by an amount equal to the Ge X-ray photon energy. Therefore, a new peak will appear in the response function that

is located at a distance equal to the energy of the X-ray below the FEP. These peaks are labelled as X-ray escape peaks and tend to be most prominent at low incident gamma-ray energies. The escape mechanism from the detector is shown in Fig. 3.5.

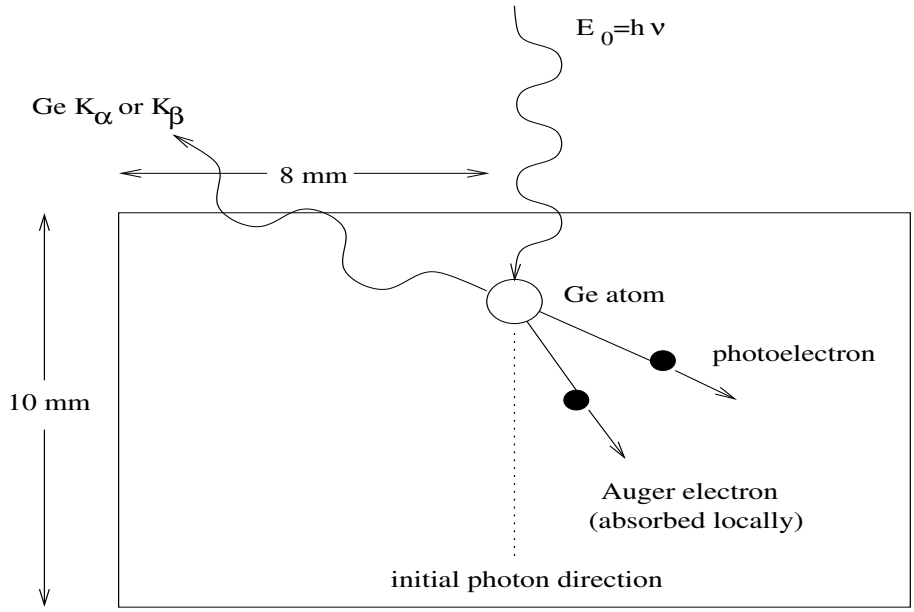

Figure 3.5: *Ge X-ray escape from the detector.*

In this investigation, escape peaks due to ^{241}Am gamma-rays were expected at about 49.6 keV (*i.e.* E_0 - E_{K_α} of Ge) and 48.5 keV (*i.e.* E_0 - E_{K_β} of Ge) as seen in Figs. 3.2-3.4. Tb and Ba X-ray escape peak energies can also be calculated easily.

3.2.3 Photoelectron Escape

Photoelectrons are charged particles, and contrary to Ge X-rays, which suffer complete absorption or escape, they deposit a part of their energy by inelastic

collisions before they escape from the detector. The escape mechanism from the detector is shown in Fig. 3.6.

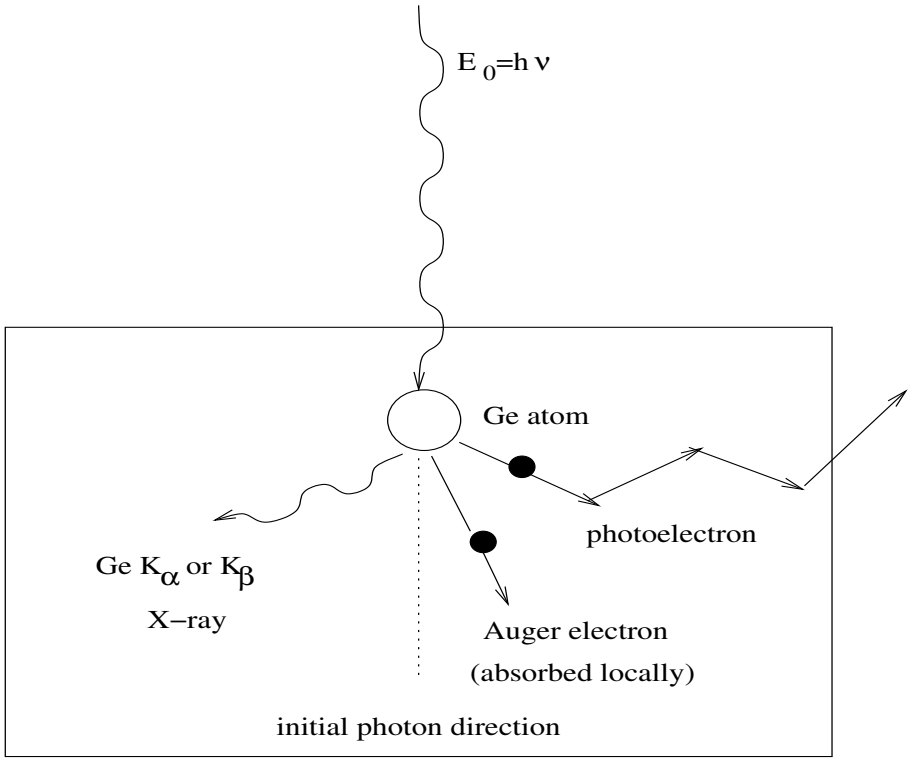

Figure 3.6: *Photoelectron escape from the detector.*

However, the fate of the Ge X-ray (or Auger electron) produced in the same interaction plays an important role regarding how and where the photoelectron escape contributes to the response function. It is clear that there are two possibilities for the X-ray: absorption or escape. If the X-ray is absorbed, the partial energy deposition by the photoelectron is expected to produce a component that starts around 11.1 keV (E_K^b) and extends up to E_0 (that is, FEP). On the other hand, if the X-ray escapes, the energy deposited by the photoelectron may vary from the minimum to its maximum energy $E_{pe} = E_0 - E_K^b$. The energies of the

photoelectrons of ^{241}Am, Tb and Ba were 48.4 keV, 33.1 keV and 20.9 keV, respectively. Figures 3.2-3.4 show the photoelectron escape component for ^{241}Am, Tb and Ba.

3.2.4 Compton-Scattered Radiation Escape

Compton continuum is the result of partial deposition of the incident photon's energy. The most probable mechanism for the escape of incident photons after partial energy deposition was a single 180° Compton scattering. Since the mean free paths of ^{241}Am, Tb and Ba photons were about 1.1 mm, 0.39 mm and 0.16 mm, respectively, as compared to 10 mm detector thickness, a single 180° inelastic scattering allowed the shortest path for the escape of the collimated photons. 180° Compton escape mechanism from the detector is shown in the Fig. 3.7.

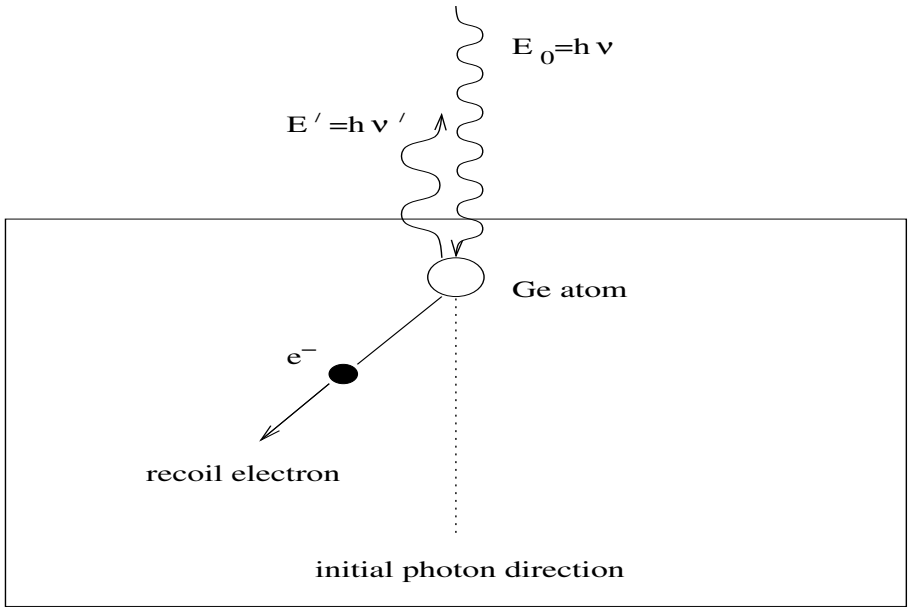

Figure 3.7: *180° Compton escape from the detector.*

Assuming scattering from free electrons, one can obtain the maximum energy of recoil electron, *i.e.* Compton edge, of ^{241}Am from Eq. (2.10) which gives $E_{e^-} = 11.3$ keV for $E_0 = 59.5$ keV. This means that the escape component is expected at approximately 11.3 keV, which is about 48.2 keV below the FEP. The energies of Compton recoil electrons and Compton scattered X-rays of Ba and Tb for 180° scattering were 3.6, 6.5 keV and 28.4, 37.7 keV, respectively.

3.2.5 Multiple Compton Scattering Followed by Photoelectric Absorption

Multiple scattering followed by photoelectric absorption plays an important role in energy deposition in a detector. Especially in the case of multiple inelastic collisions, energy is deposited through successive processes ending with the complete absorption of the photon. The location of all these interactions, the fate of recoil electrons, photoelectron and Ge X-ray (or Auger electrons) will thus be important. The total fractional probability of inelastic and elastic collisions is about 0.12, 0.07 and 0.04 at the incident energies 59.5, 44.2 and 32 keV considered in this thesis.

Photons undergoing multiple scattering of either kind or a combination of the two (Compton-coherent-Compton or coherent-Compton-coherent, etc) of the two with an eventual photoabsorption were studied. Fig. 3.8 shows an example of double Compton scattering followed by photoelectric absorption. The contribution of these processes to the response function will be presented in Chapter 5.

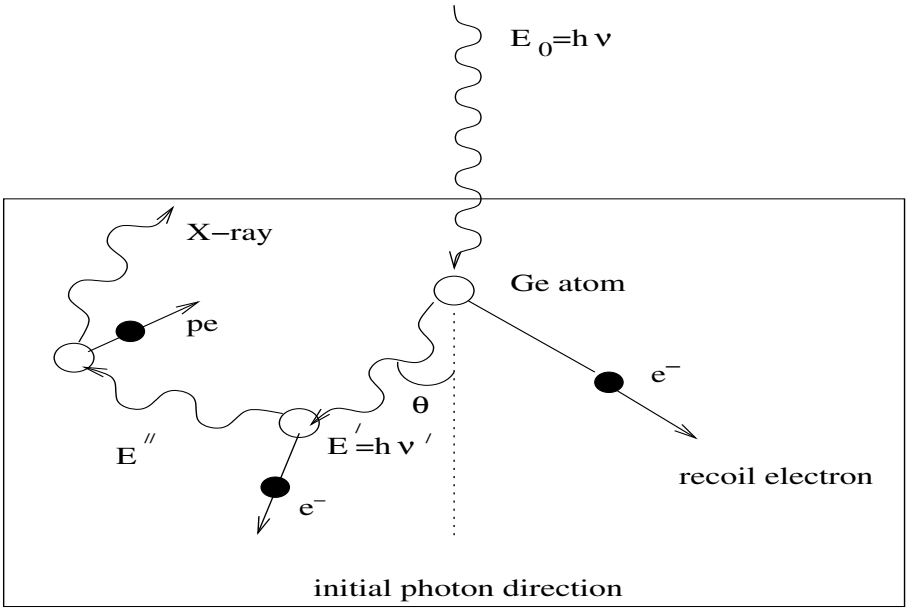

Figure 3.8: *Multiple Compton scattering inside the detector.*

CHAPTER 4

MONTE CARLO SIMULATIONS

4.1 Basic Principles

Our Monte Carlo simulations were based on the interactions between photons and Ge atom. Since all relevant probabilities were fairly known for the elementary events in the life history of a photon, the Monte Carlo method was applicable. Its technique consisted following each of a large number of photons from the source throughout its life history to its death. The history of secondary photons and electrons are also followed from an interaction site until they are absorbed inside the detector or until they escape.

Random numbers were generated and used for sampling the initial photon direction, the point of entrance of the photon into the detector, the distance between interactions, the type of interaction, the scattering angle and energy of the photon. Similar procedures were applied for the secondary photons and the electrons.

Space coordinates (x, y, z) were used to determine the position of each photon and its direction coordinates, *i.e.* direction cosines, (u, v, w) for its flight [40]:

$$u = \cos\alpha \tag{4.1}$$

$$v = \cos\beta \tag{4.2}$$

$$w = \cos\gamma \tag{4.3}$$

where $0 \leq \alpha, \beta, \gamma \leq \pi$ and on this range the cosines assume all values on the range $-1 \leq u, v, w \leq 1$. Also the direction coordinates (u, v, w) were regarded as defining a point on the unit sphere $u^2 + v^2 + w^2 = 1$ in direction space U, V, and W.

In order to determine the location of the first collision, we made use of the attenuation law

$$dn = -(dl)nN\sigma \tag{4.4}$$

where n is the number of particles in the beam, N is the numerical density (target particles per cm^3, σ is the cross section and dl is the thickness, and

$$n = n_0 \exp(-N\sigma l) \tag{4.5}$$

represents the number of particles remaining in the beam after traversing a distance l in the detector material, n_0 being the number of particles in the beam at $l = 0$. It is supposed that

$$p(l)dl = [\exp(-N\sigma l)]N\sigma(dl) \tag{4.6}$$

is the probability for a collision between l and $l + dl$, and

$$P(l) = \int_0^l \exp(-N\sigma l)N\sigma(dl) = 1 - \exp(-N\sigma l) \tag{4.7}$$

is the corresponding probability distribution function for a first collision at distance $\leq l$.

The average distance λ to first collision was defined as the first moment of the function $p(l)$, i.e.

$$\lambda = \int_0^\infty lp(l)dl = \int_0^\infty \exp(-N\sigma l)N\sigma l(dl) = 1/N\sigma \tag{4.8}$$

and was called the mean free path for the process at this energy.

It follows that the Monte Carlo determination of distance l from an arbitrary point of departure to first collision, assuming the medium homogeneous and infinite must be

$$r = P(l) = 1 - \exp(-l/\lambda) \tag{4.9}$$

or

$$l = -\lambda \ln(1 - r) \tag{4.10}$$

where r is a random number. Since $1 - r$ is equidistributed on $0 \leq r \leq 1$, we may use simply

$$l = -\lambda \ln r. \tag{4.11}$$

The final direction coordinates of a Ge X-ray, an electron or a scattered photon in the laboratory system are given by [40]

$$u' = \frac{(bcwu - bdv)}{\sqrt{(1 - w^2)}} + au \tag{4.12}$$

$$v' = \frac{(bcwv - bdu)}{\sqrt{(1 - w^2)}} + av \tag{4.13}$$

$$w' = -bc\sqrt{(1 - w^2)} + aw \tag{4.14}$$

where

$$a = \cos\theta \tag{4.15}$$

$$b = \sin\theta = \sqrt{(1 - a^2)} \tag{4.16}$$

$$c = \cos\delta \tag{4.17}$$

$$d = \sin\delta = (\text{sign of } \delta)\sqrt{(1 - c^2)} \qquad -\pi \leq \delta \leq \pi \tag{4.18}$$

where θ is the scattering angle (or emission angle for Ge X-rays and electrons) with direction of the incident line of flight, and δ is the azimuthal angle uniformly distributed on $-\pi \leq \delta \leq \pi$.

When $|w|$ is too close to unity, the following equations are used:

$$u' = bc \tag{4.19}$$

$$v' = bd \tag{4.20}$$

$$w' = aw. \tag{4.21}$$

When the new direction cosines are found for the scattered photon (or emitted X-ray), the location of the next interaction can be found by

$$x' = x + u'l \tag{4.22}$$

$$y' = y + v'l \tag{4.23}$$

$$z' = z + w'l \tag{4.24}$$

where l is given in Eq. (4.11). In the case of a photoelectron, l is replaced by the distance between successive inelastic collisions.

4.2 Monte Carlo Program

The program followed the history of a large number of photons (typically five million). First initial direction coordinates (u, v, w) and the entrance point of the photon were determined by generating a random number. Then, by using the mean free path of the photon in Ge [31], the coordinates of the first interaction point (x, y, z) was determined. If the location of the first interaction of the photon was outside the detector, the photon was assumed to escape without any interaction and the history of that photon was terminated. This event was named as the primary photon escape. However, if the location of the first interaction of the photon was inside the detector, the photon was assumed to have undergone an interaction.

The simulations were based on three primary interactions, namely, the photoelectric absorption, Compton and coherent scattering between the incident photons and the atoms of the detector material. Using the cross-sections [31, 41, 42] of these interactions, the first event was sampled by the aid of a random number. Scattered photons, recoil electrons, Ge X-rays, photoelectrons, and Auger electrons were all accounted for in the program.

As it was mentioned before, in the case of photoelectric effect, a photoelectron is produced along with the emission of a characteristic X-ray or ejection of an Auger electron. By the use of a random number, X-ray or Auger electron emission was chosen. Again, by generating a random number, the type of the characteristic X-ray was sampled. The history of photoelectrons, K_α and K_β X-rays with

the energies of 9.88 keV and 10.98 keV and Auger electrons were followed. The intensities of K_α and K_β X-rays were 0.884 and 0.116 [41] relative to the total K X-rays and the mean free paths were 45 μm and 60 μm, respectively. If the interaction point of a K_α or K_β X-ray was inside the detector, it was assumed to be absorbed. Otherwise, an event for K_α or K_β X-ray escape was recorded. Moreover, the escape of X-rays from the side or top surface of the detector was considered. If both the photoelectron and K_α or K_β X-ray escaped together, it was recorded as a coincidence event. If the photoelectron did not escape but K_α or K_β X-ray escaped, total X-ray escape without coincidence event was recorded. If both the photoelectron and K_α or K_β X-ray stayed inside the detector, a full-energy peak event was recorded. All other X-rays from higher shells were assumed to be absorbed completely. As the Auger electrons have small energy which leads to small mean free paths, they were assumed to be absorbed completely. While mean free paths for scattered photons and Ge X-rays were used to determine if an escape event had occurred, range of photoelectron [43, 44], divided into logarithmically decreasing path lengths, was employed for the transport of photoelectron undergoing successive inelastic collisions. For each scattering event, an average angle was found using [45]

$$\cos\theta = [(E_{n+1}/E_n)(E_n + 2m_0c^2)/(E_{n+1} + 2m_0c^2)]^{0.3Z} \tag{4.25}$$

where $E_{n+1} = kE_n$ with $k = 2^{-1/m}$. Here m is the number of steps for which half of the energy is lost. In our simulations, we used $m = 25$ with a total of 250 collisions. This corresponds to an energy loss of 1.3 keV during the first

collision of 48.4 keV photoelectrons produced by 59.5 keV ^{241}Am photons. In the case of Tb and Ba, the energy loss in the first collision were 0.9 keV and 0.57 keV, respectively. All events and the resulting amount of energy deposited were recorded.

The history of the photoelectrons, with energy of 48.5 keV and a range of 13 μm for Am, energy of 44.22 keV and a range of 6.7 μm for Tb, and energy of 32 keV a range of 3.2 μm for Ba, was followed using the angular distribution which is proportional to $\sin^2\theta$ for nonrelativistic electrons.

In the case of Compton (inelastic) scattering, by generating a random number, the angle of scattering was determined using the Klein-Nishina formula for differential cross-section which is corrected by the scattering factor. The final energy of the Compton scattered photon was determined by taking into account the electron momentum distribution (*i.e.* Compton profile) of the electrons. The energies of the recoil electrons were calculated from Eq. (2.8) and were assumed to be absorbed locally. Using cross-sections, the mean free path of the photon was calculated and so the location of the next interaction was determined. If the interaction point was outside the detector, the incident photon was said to have escaped after depositing only a part of its energy. Otherwise, the second interaction, having the new energy obtained from Eq. (2.13) was considered.

In the case of coherent scattering, the angle of scattering was determined using the Thompson cross-section formula corrected by the form factor, Eq. (2.14), along with a random number. For both inelastic and elastic collisions the azimuthal angle was sampled from a uniform distribution.

CHAPTER 5

RESULTS AND DISCUSSION

In this chapter, each pertinent component of the ^{241}Am gamma-ray, and Tb and Ba X-ray spectra will be examined in the light of the information obtained from the Monte Carlo simulations. The predicted features of the response functions will be compared with the measured spectra which were analyzed using the peak-fitting program. All FEPs and their X-ray escape peaks were fitted by individual Gaussian distributions. Compton escape was represented, approximately, by a Gaussian distribution. Exponentially modified Gaussian distribution was used to find the net counts under the photoelectron escape component. In the following sections, the role of Ge X-rays, photoelectrons and recoil electrons will be discussed in detail.

5.1 Full-Energy Peak

In order to record the events yielding FEP in our Monte Carlo program, we imposed the coincidence condition that Ge X-ray or Auger electron was absorbed in the detector and the photoelectron deposited all of its energy through inelastic collisions. However, the K-shell fluorescence yield of Ge is only $\omega_K = 0.554$ and nonradiative decay with the ejection of Auger electrons is almost equally

probable. Monte Carlo program takes this fact into account with the assumption that these electrons deposit all of their energy (< 11 keV) in the vicinity of the interaction site. The single points in Figs. 5.1, 5.6 and 5.11 at E_0=59.5 keV, 44.2 keV and 32 keV represent the total number of FEP events which will be used to evaluate various escape fractions. For a collimator radius of 3 mm and for five million photons, we found that about 97% of the photons deposit full energy inside the detector.

5.2 Ge X-Ray Escape

X-ray escape peaks are the result of the escape of Ge K_α or K_β X-ray in coincident with the full deposition of energy by the accompanying photoelectron. Using the K X-ray intensity ratio and the mean free paths, the Monte Carlo program followed the history of Ge K_α and K_β separately. X-ray escape or absorption events were recorded along with the information regarding full or partial energy deposition by the photoelectron. Therefore, while we were able to estimate the fractional escape ratio for both Ge K_α and K_β X-rays, we presented, for the sake of simplicity, the total number of X-ray escape events by a single point at $E_0 - E_X$=48.4 keV, 33.1 keV and 20.9 keV in Figs. 5.2, 5.7 and 5.12.

5.3 Photoelectron Escape

In any Monte Carlo study of a semiconductor detector, the transport and thus the energy deposition of a photoelectron is of great importance. Each photoelectric absorption event results in the ejection of a photoelectron, and the mechanism

by which it loses its energy in the detector needs to be studied as realistically as possible. Photoelectron escape after partial energy deposition in coincident with Ge X-ray escape has, to our knowledge, never been studied before. A comparison of Figs. 5.1 and 5.2 reveals that while the sloping shape of the escape components are essentially similar, the overall intensities are different (3:1 for ^{241}Am) in favor of the case with Ge X-ray absorption. What is more interesting here is the finding that the photoelectron escape components for three different incident photon energies, Figs. 5.6 and 5.7, 5.11 and 5.12, show similar behavior, that is they all have a slope. The predicted slopes are presented in Table 5.1. An increasing slope was observed with decreasing energy. The predicted escape fractions, even when the two mechanisms are taken into account, were always underestimated compared to the measured values.

Table 5.1: Predicted slopes of photoelectron escape component.

	^{241}Am	Tb	Ba
Ge X-ray absorbed	-0.043	-0.060	-0.099
Ge X-ray escaped	-0.029	-0.050	-0.077

5.4 Compton Scattering Followed by Photoelectric Absorption

The most important advantage of a Monte Carlo simulation is the fact that the details of the interaction mechanisms between the incident photons and the detector atoms, as well as, between the secondary photons (Ge X-rays), charged

particles (photoelectrons, Auger and recoil electrons) and the detector material can be obtained simply by recording the relevant information.

Even though all recoil electrons were assumed to lose their energy in the vicinity of the collision site, we recorded their energy separately and treated them as if they escaped without any interaction. We must keep in mind that the recoil energies in this case are smaller than the 180° escape case, and since, after single, double *etc.* inelastic scattering photoelectric absorption occurs, these events are expected on the low energy side of the full-energy peak. Figures 5.3, 5.8 and 5.13 clearly show two distinct structures, marked as single+multiple and multiple scattering. In the region marked as single, in Fig. 5.3, there can be multiple scattering events at small angles, but in the double and multiple collision regions we expect only multiple scattering. The reason for this is that the lower limit of the single+multiple scattering region is at about 48.3 keV which corresponds to the energy of the photon after a single 180° scattering. That is, the contribution of recoil electron is about 11.2 keV. The lower limit of the multiple-scattering region is at about 40.6 keV. This corresponds to two successive 180° scattering. Figures 5.4, 5.9 and 5.14 show the recoil electron contribution in the case of Ge X-ray escape. In Fig. 5.4, the events around 37 keV were interpreted as single+multiple scattering followed by the photoelectric absorption with Ge X-ray escape. For example, a single 180° scattering would bring the photon very close to the front surface. If the photon then undergoes photoelectric absorption, the Ge X-ray thus produced has a good chance to escape. In this way, the energy deposited would be $E_0 - E_{re}(180°) - E_x$=59.5-11.2-11.1=37.2 keV. It is interesting to note that

the shape of the recoil electron spectrum (Fig. 5.4) is similar to the experimental result (Fig. 3.2), suggesting that similar collisions might be taking place before the photons enter the detector but these effects were minimized.

5.5 180° Compton Escape

Figures 5.5, 5.10 and 5.15 show the 180° Compton escape spectra of ^{241}Am, Tb and Ba for five million incident photons. The full-width-at-half-maximum (FWHM) for each spectrum is shown in Table 5.2. Both the measured and predicted spectra were fitted using a Gaussian distribution. Good agreement was obtained for all cases considered. Since inelastic scattering cross-section for the energy range considered was only about 10%, the probability of multiple scattering followed by escape is quite low. This is verified in Figs. 5.5, 5.10 and 5.15 because any significant amount of multiple scattering would cause a prominent continuum in the escape peak.

Table 5.2: Experimental and predicted FWHM (in keV) of Compton escape component.

	Experiment	Monte Carlo
^{241}Am	3.75±0.11	3.86
Tb	2.99±0.05	2.79
Ba	1.65±0.10	1.90

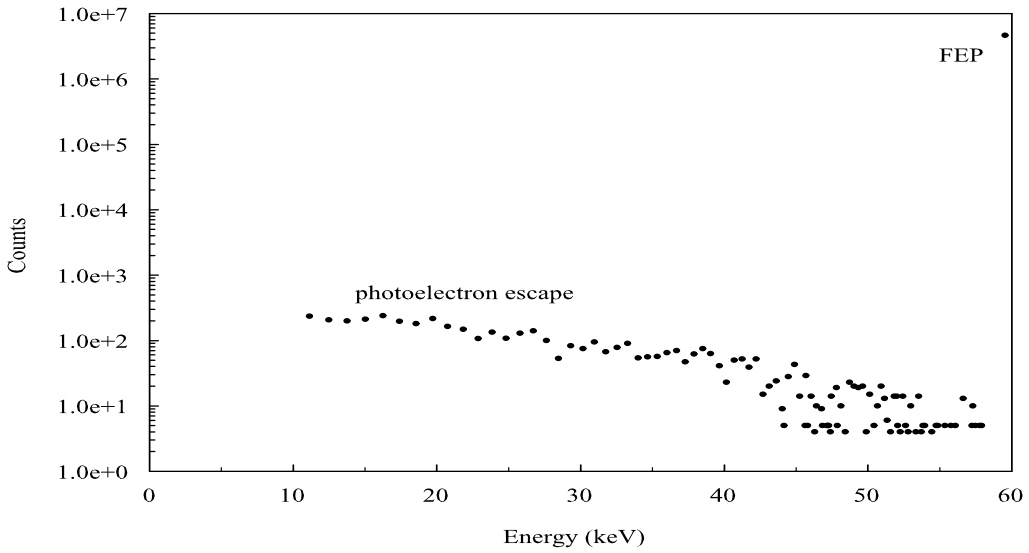

Figure 5.1: *Photoelectron escape in coincident with Ge X-ray absorption for incident* ^{241}Am *gamma rays.*

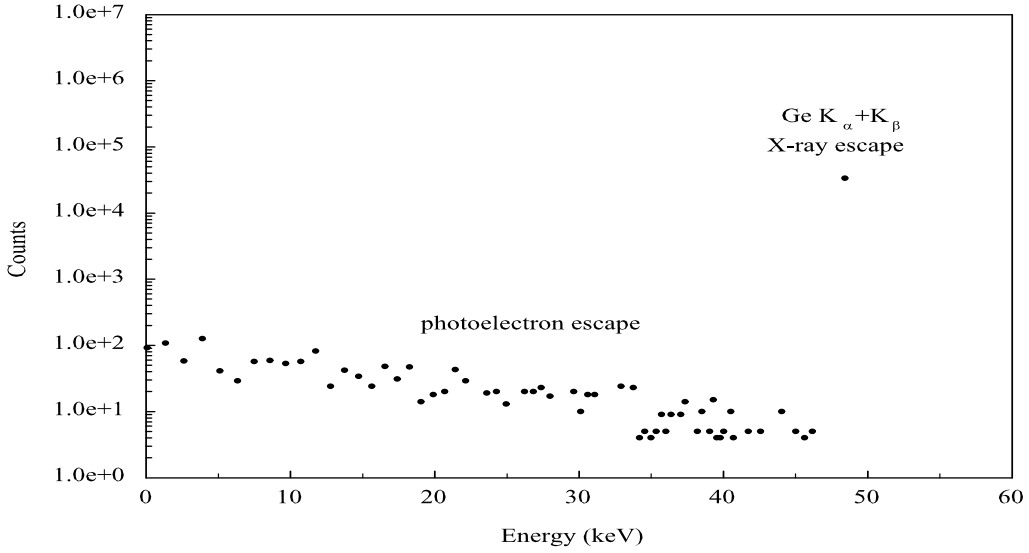

Figure 5.2: *Photoelectron escape in coincident with Ge X-ray escape for incident* ^{241}Am *gamma rays.*

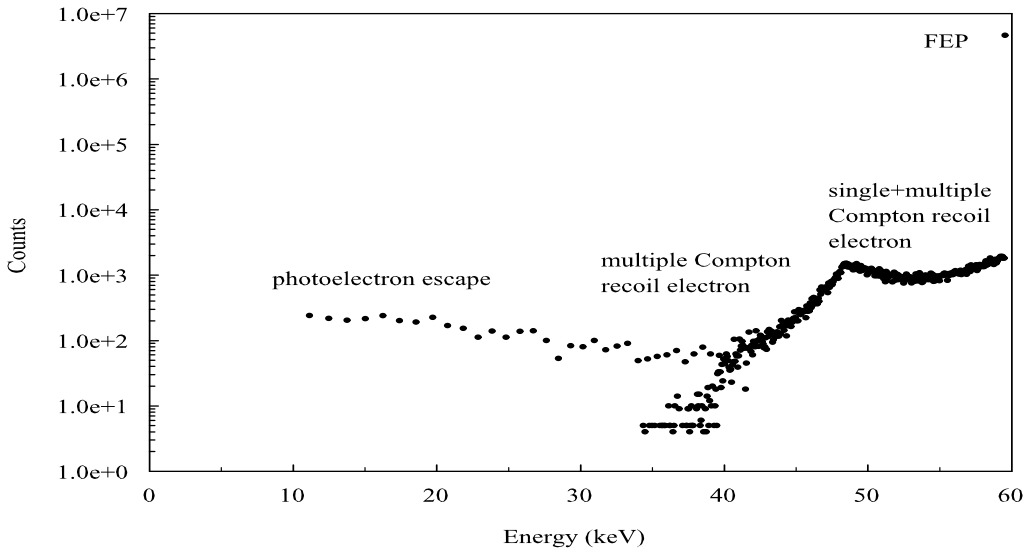

Figure 5.3: *Single+multiple Compton scattering followed by photoelectric absorption with Ge X-ray absorption for incident* ^{241}*Am gamma rays.*

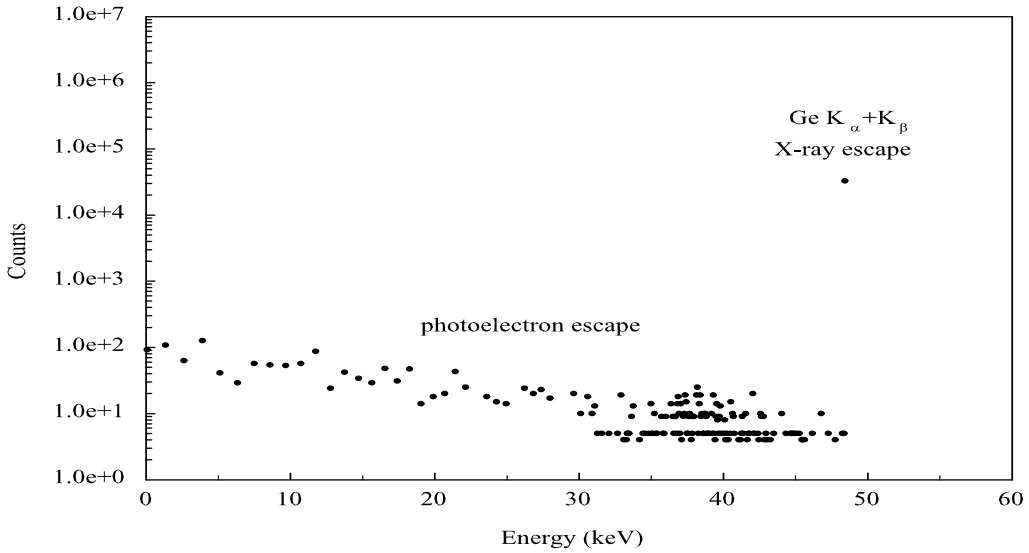

Figure 5.4: *Single+multiple Compton scattering followed by photoelectric absorption with Ge X-ray escape for incident* ^{241}*Am gamma rays.*

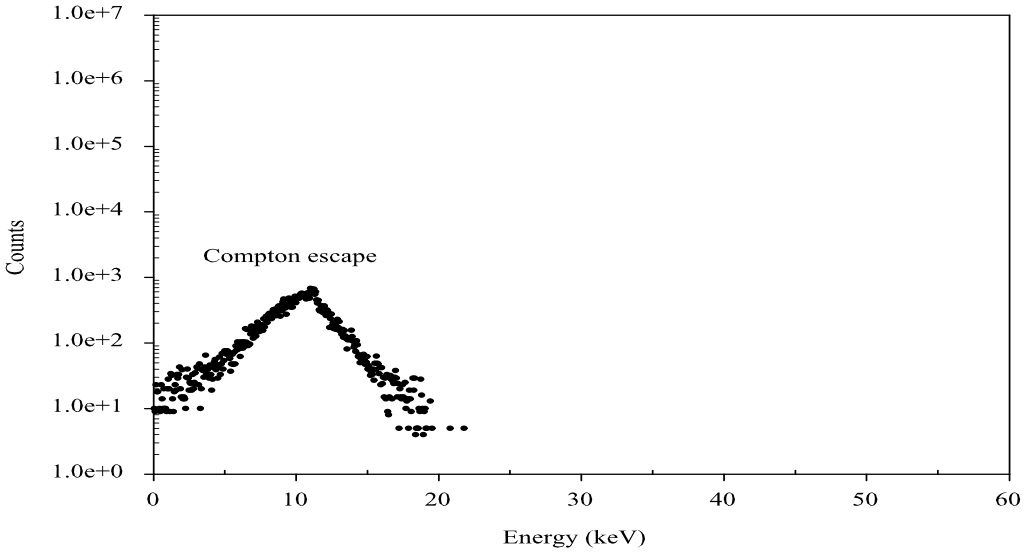

Figure 5.5: 180° *Compton escape for incident* ^{241}Am *gamma rays.*

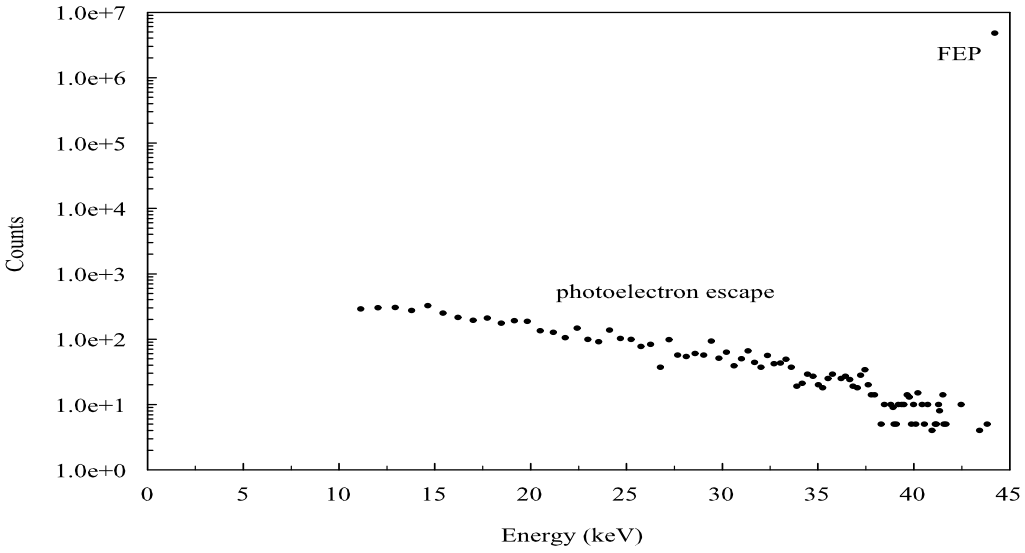

Figure 5.6: *Photoelectron escape in coincident with Ge X-ray absorption for incident Tb X-rays.*

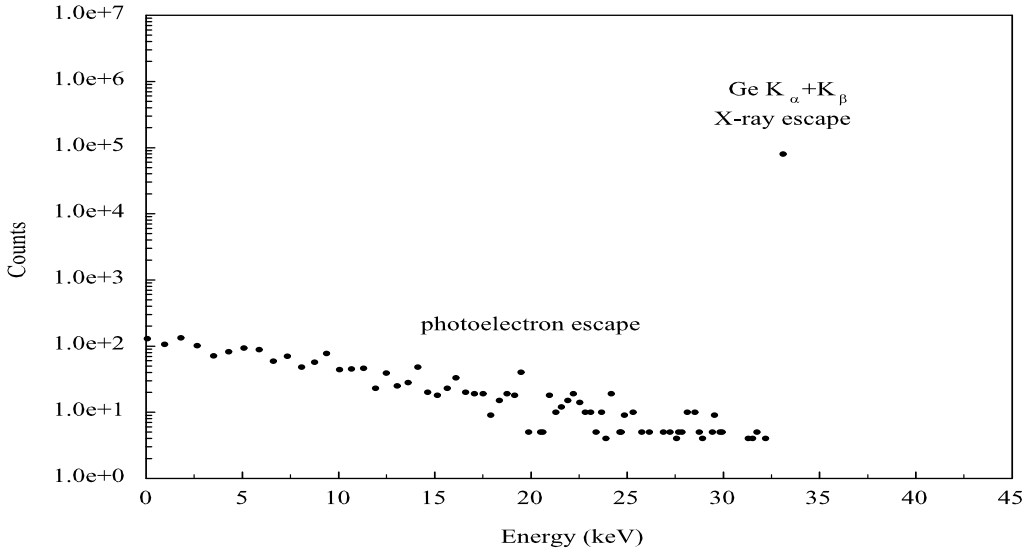

Figure 5.7: *Photoelectron escape in coincident with Ge X-ray escape for incident Tb X-rays.*

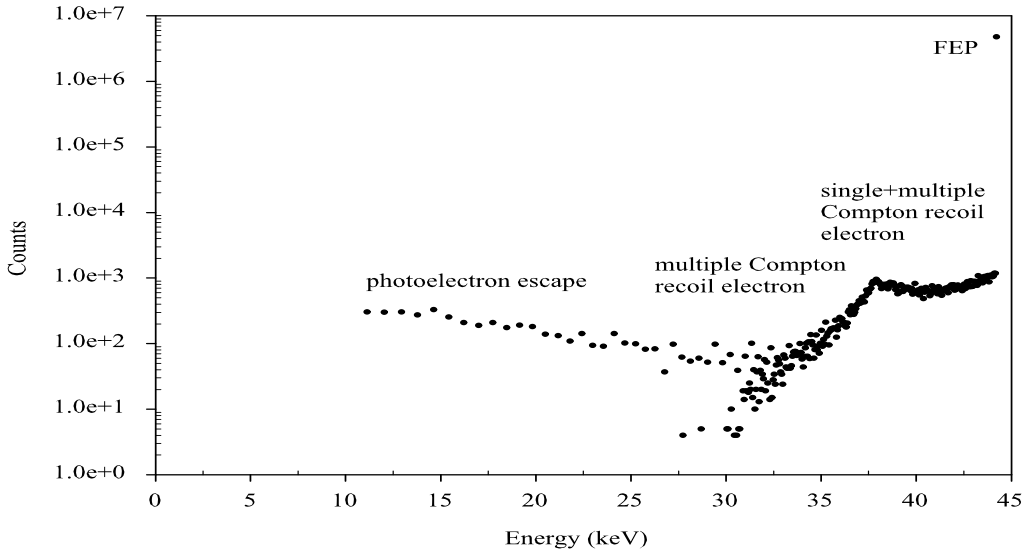

Figure 5.8: *Single+multiple Compton scattering followed by photoelectric absorption with Ge X-ray absorption for incident Tb X-rays.*

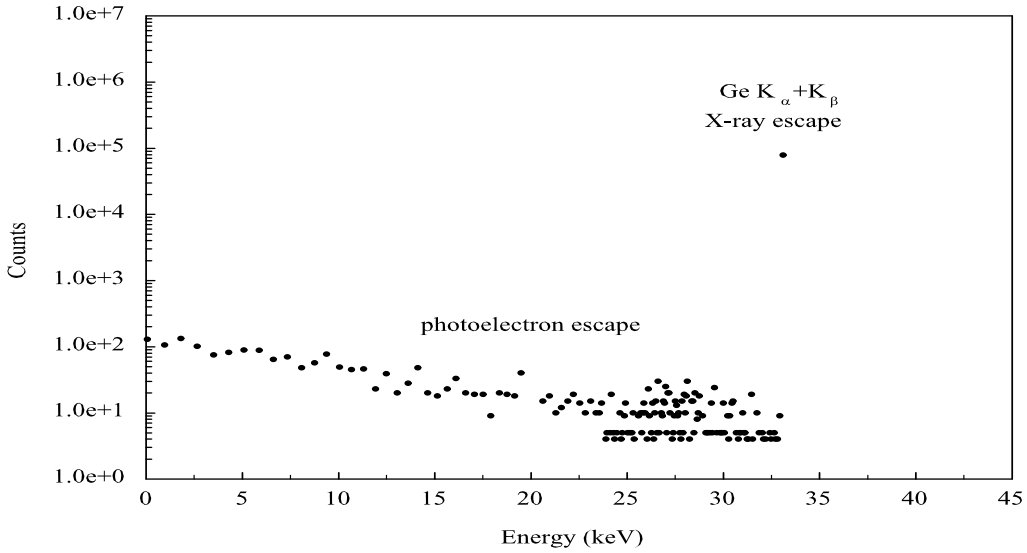

Figure 5.9: *Single+multiple Compton scattering followed by photoelectric absorption with Ge X-ray escape for incident Tb X-rays.*

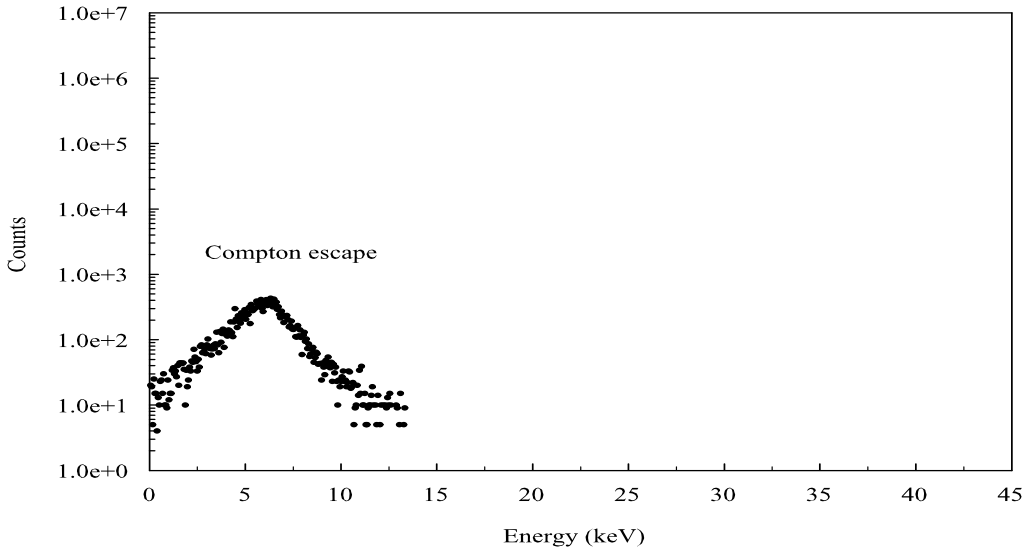

Figure 5.10: 180° *Compton escape for incident Tb X-rays.*

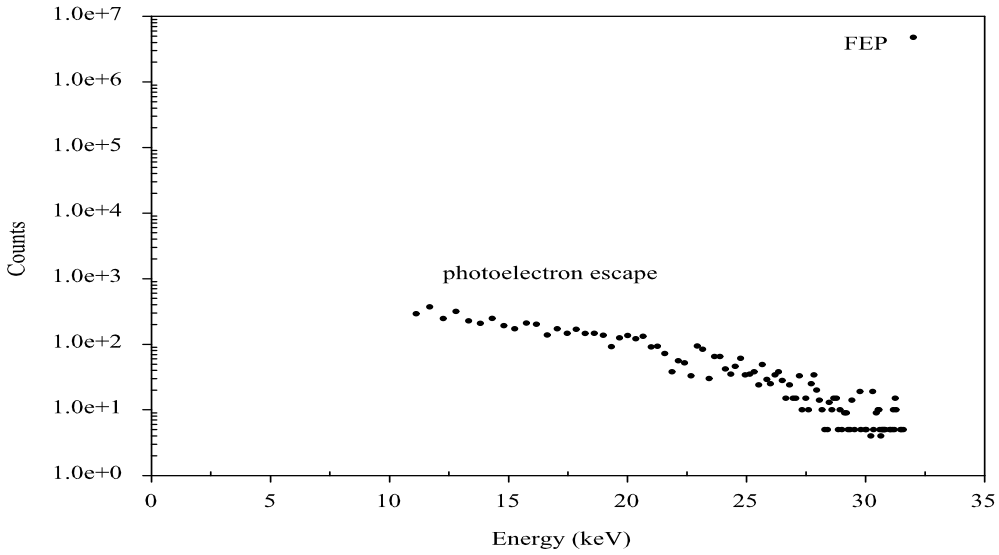

Figure 5.11: *Photoelectron escape in coincident with Ge X-ray absorption for incident Ba X-rays.*

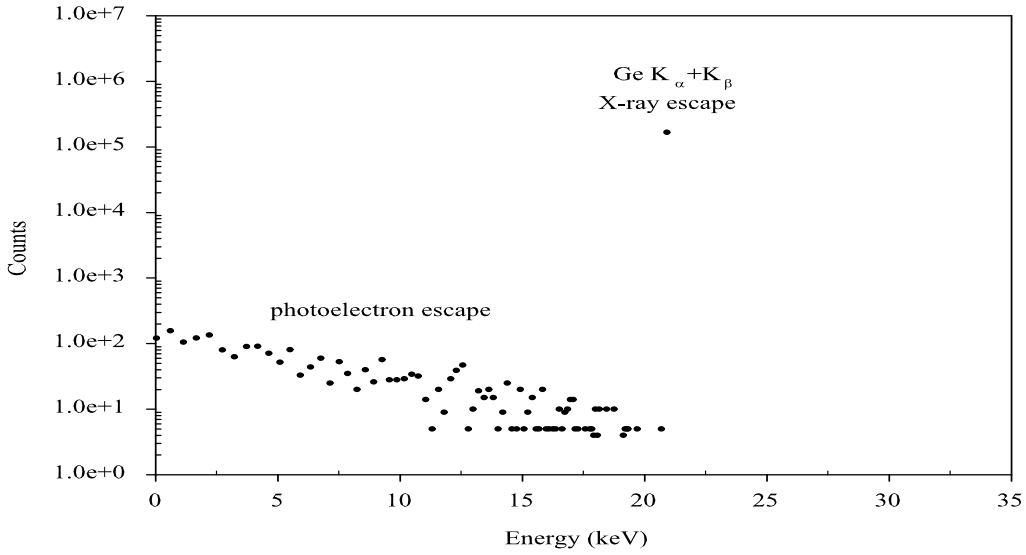

Figure 5.12: *Photoelectron escape in coincident with Ge X-ray escape for incident Ba X-rays.*

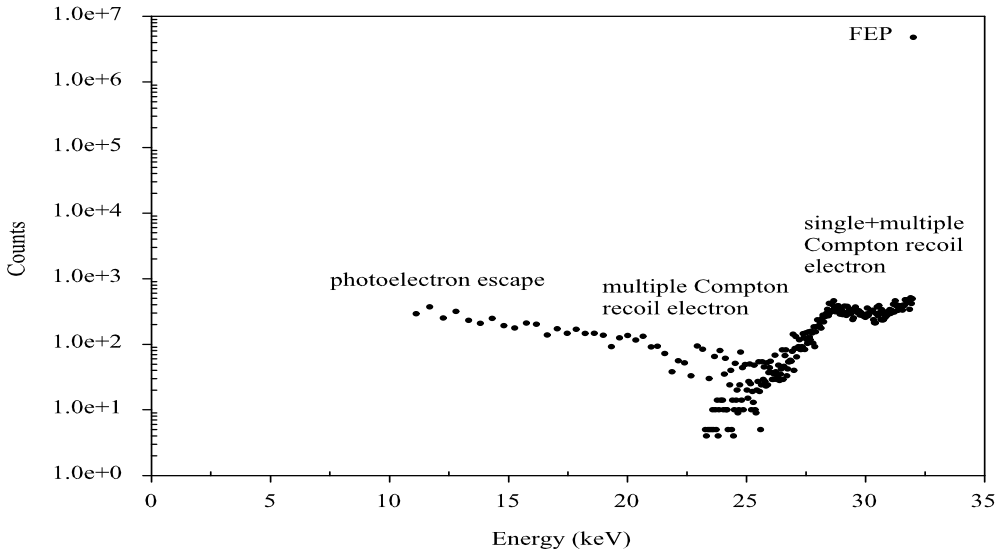

Figure 5.13: *Single+multiple Compton scattering followed by photoelectric absorption with Ge X-ray absorption for incident Ba X-rays.*

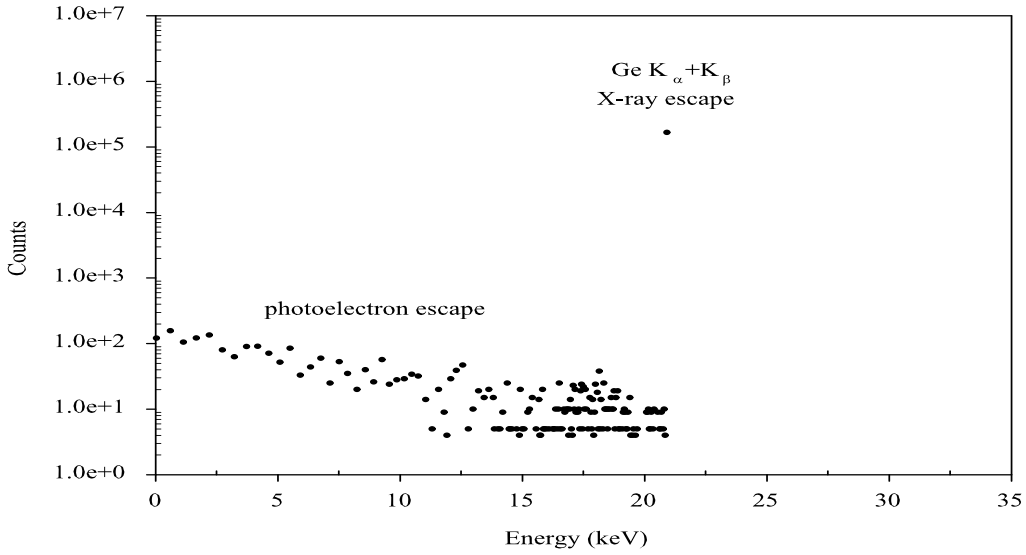

Figure 5.14: *Single+multiple Compton scattering followed by photoelectric absorption with Ge X-ray escape for incident Ba X-rays.*

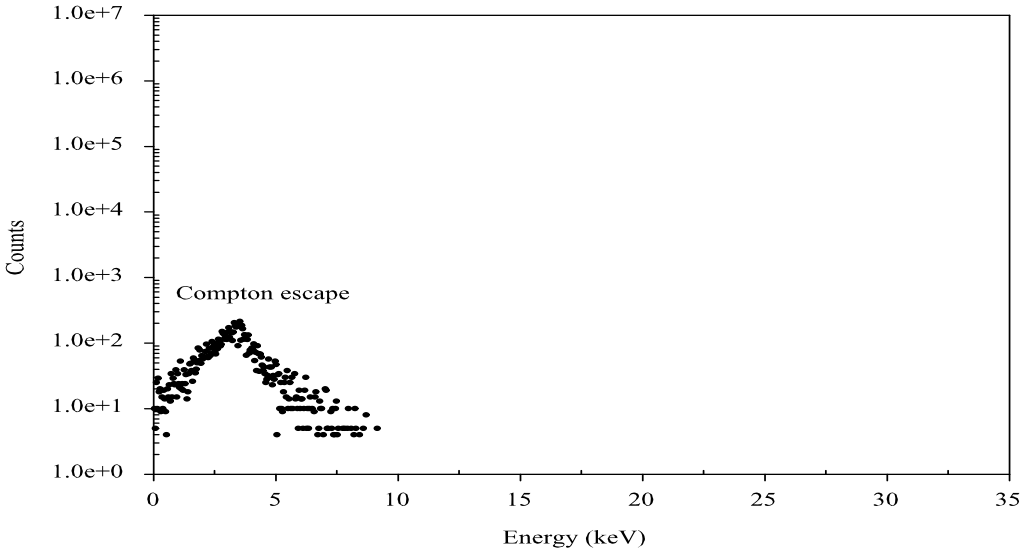

Figure 5.15: 180° *Compton escape for incident Ba X-rays.*

CHAPTER 6

CONCLUSION

In this thesis, we investigated the escape/absorption of photons, photoelectrons, Auger electrons, recoil electrons and X-rays of the detector material for ^{241}Am gamma-ray, Tb and Ba X-rays, and analyzed each mechanism both qualitatively and quantitatively.

Particular attention was given to the photoelectrons and recoil electrons produced in the detector. Monte Carlo program was improved to study the transport of photoelectrons and energy deposition by recoil electrons. For photoelectrons, two mechanisms were identified: one with Ge X-ray escape and the other with absorption. Energy spectrum of both mechanisms have slopes. Recoil electron's contribution to spectrum, after single or multiple Compton scattering followed by photoelectric absorption was studied. Single and multiple scattering were clearly identified in the predicted spectra. Predicted FWHM of 180° Compton escape were compared with experimental spectra. Good agreement was seen.

Predicted fractional ratios for the escape of Ge X-rays (Kα and Kβ), 180° Compton scattered photons and photoelectrons were obtained and compared with the ones before the improvements in the Monte Carlo program. Consistent results were observed for X-rays and Compton scattered photons. However, the predicted

ratios for photoelectron escape were even lower than the previous values, because a much more realistic transport mechanism was used. This is because, previously we treated the photoelectron like a photon, and used its range as the distance to the first interaction. If the interaction point was inside, the photoelectron was assumed to have deposited all of its energy, otherwise an escape event has occurred with no energy deposition. In the present model partial deposition through successive collisions was allowed, which reduced the escape probability.

REFERENCES

[1] A. Sood, R.P. Gardner, Nucl. Instrum. Methods B 2004; **213**: 100.

[2] M.C. Lépy, J. Plagnard, P. Stemmler, G. Ban, L. Beck, P. Dhez, X-Ray Spectrom. 1997; **26**: 195.

[3] J.L. Campbell, J.A. Maxwell, T. Papp, G. White, X-Ray Spectrom. 1997; **26**: 223.

[4] T. Papp, J.L. Campbell, D. Varga, G. Kalinka, Nucl. Instrum. Methods A 1998; **412**: 109.

[5] T. Papp, J.L. Campbell, X-Ray Spectrom. 2001; **30**: 77.

[6] S. Goto, Nucl. Instrum. Methods A 1993; **333**: 452.

[7] J.X. Wang, J.L. Campbell, Nucl. Instrum. Methods B 1991; **54**: 499.

[8] J.L. Campbell, L. McDonald, T. Hopman, T. Papp, X-Ray Spectrom. 2001; **30**: 230.

[9] S. Goto, J. Synchroton Radiat. 1998; **5**: 880.

[10] H.J. He, T.W. Zhang, R.C. Shang, S.D. Xu, Nucl. Instrum. Methods A 1998; **272**: 847.

[11] R.P Gardner, A.M. Yacout, J. Zhang, K. Verghese, Nucl. Instrum. Methods A 1986; **242**: 399.

[12] Y. Jin, R.P. Gardner, K. Verghese, Nucl. Instrum. Methods A 1986; **242**: 416.

[13] A.M. Yacout, R.P. Gardner, K. Verghese, Nucl. Instrum. Methods A 1986; **243**: 121.

[14] M.V. Gysel, P. Lemberge, P.V. Espen, X-Ray Spectrom. 2003; **32**: 139.

[15] P. Sangsingkeow, K.D. Berry, E.J. Dumas, T.W. Raudorf, T.A. Underwood, Nucl. Instrum. Methods A 2003; **505**; 183.

[16] B.G. Lowe, Nucl. Instrum. Methods A 2000; **439**: 247.

[17] J.L. Campbell, G. Cauchon, M.C. Lépy, L. McDonald, J. Plagnard, P. Stemmler, W.J. Teesdale, G. White, Nucl. Instrum. Methods A 1998; **418**: 394.

[18] T. Papp, X-Ray Spectrom. 2003; **32**: 00.

[19] M.C. Lépy, J.L. Campbell, J.M. Laborie, J. Plagnard, P. Stemmler, W.J. Teesdale, Nucl. Instrum. Methods A 2000; **439**: 239.

[20] L.H. Christensen, X-Ray Spectrom. 1979; **8**: 146.

[21] C. Can, S.Z. Bilgici, X-Ray Spectrom. 2003; **32**: 276.

[22] L.J. Martin, P.A. Burns, Nucl. Instrum. Methods A 1992; **312**: 146.

[23] S. Pašić, K. Ilakovac, Nucl. Instrum. Methods A 1998; **405**: 45.

[24] M.C. Lépy, J. Plagnard, L. Ferreux, Nucl. Instrum. Methods A 2003; **505**: 290.

[25] F. Scholze, M. Procop, X-Ray Spectrom. 2001; **30**: 69.

[26] A.G. Karydas, Ch. Zarkadas, A. Kyriakis, J. Pantazis, A. Huber, R. Redus, C. Potiriadis, T. Paradellis, X-Ray Spectrom. 2003; **32**: 93.

[27] C. Can, X-Ray Spectrom. 2003; **32**: 280.

[28] E. Yılmaz, C. Can, X-Ray Spectrom. In press.

[29] E. Yılmaz, R. Peköz, C. Can, Submitted.

[30] J.M O'Meara, J.L Campbell, X-Ray Spectrom. 2004; **33**: 146.

[31] http://physics.nist.gov/cgi-bin/Xcom/xcom3_1.

[32] http://www.cea.com/cai/augtheo/energies.htm

[33] R.E. Lapp, H.L. Andrews, *Nuclear Radiation Physics*, Prentice-Hall, Inc., New Jersey, 1972.

[34] C.F. Knoll, *Radiation Detection and Measurement*, John Wiley and Sons, Inc., USA, 2001.

[35] O. Klein, Y.Z. Nishina, Phys. 1929; **52**: 853.

[36] D.T. Cromer, J. Chem. Phys. 1969; **50**(11): 4857.

[37] J.H. Hubbell, Wm.J. Veigele, E.A. Briggs, R.T. Brown, D.T. Cromer,R.J. Howerton, J. Phys. Chem. Ref. Data 1975; **4**(3): 471.

[38] F. Biggs, L.B. Mendelson, J.B. Mann, Atomic Data and Nucl. Data Tables 1975; **16**: 201.

[39] R.D. Evans, *The Atomic Nucleus*, McGraw-HILL Book Company, 1969.

[40] E.D. Cashwell, C.J. Everett, *Monte Carlo Method*, Pergamon Press, 1959.

[41] E. Storm, H.I. Israel, Nucl. Data Tables A 1970; **7**: 565.

[42] W.M.J. Veigele, Atomic Data 1973; **5**: 75.

[43] T. Mukoyama, Nucl. Instrum. Methods 1976; **134**: 125.

[44] M.J. Berger, http://physics.nist.gov/PhysRefData/Star/Text/ESTAR.html

[45] B. Grosswendt, E. Waibel, Nucl. Instrum. Methods 1975; **131**: 143.